



OPEN ACCESS

EDITED BY

Sylvain Gioux,
Intuitive Surgical Sàrl, Switzerland

REVIEWED BY

Irving Bigio,
Boston University, United States
Alexandre Douplik,
Ryerson University, Canada

*CORRESPONDENCE

Anouk L. Post,
a.post@nki.nl

SPECIALTY SECTION

This article was submitted
to Biophotonics,
a section of the journal
Frontiers in Photonics

RECEIVED 08 June 2022

ACCEPTED 15 August 2022

PUBLISHED 26 September 2022

CITATION

Witteveen M, Faber DJ,
Sternborg HJCM, Ruers TJM,
van Leeuwen TG and Post AL (2022),
Opportunities and pitfalls in (sub)diffuse
reflectance spectroscopy.
Front. Photonics 3:964719.
doi: 10.3389/fphot.2022.964719

COPYRIGHT

© 2022 Witteveen, Faber, Sternborg,
Ruers, van Leeuwen and Post. This is an
open-access article distributed under
the terms of the [Creative Commons
Attribution License \(CC BY\)](https://creativecommons.org/licenses/by/4.0/). The use,
distribution or reproduction in other
forums is permitted, provided the
original author(s) and the copyright
owner(s) are credited and that the
original publication in this journal is
cited, in accordance with accepted
academic practice. No use, distribution
or reproduction is permitted which does
not comply with these terms.

Opportunities and pitfalls in (sub) diffuse reflectance spectroscopy

Mark Witteveen¹, Dirk J. Faber², Henricus J. C. M. Sternborg^{1,2},
Theo J. M. Ruers¹, Ton G. van Leeuwen² and Anouk L. Post^{1,2*}

¹Department of Surgery, The Netherlands Cancer Institute, Amsterdam, Netherlands, ²Department of Biomedical Engineering and Physics, Amsterdam UMC, University of Amsterdam, Amsterdam, Netherlands

For a long time, steady-state reflectance spectroscopy measurements have been performed so that diffusion theory could be used to extract tissue optical properties from the reflectance. The development of subdiffuse techniques, such as Single Fiber Reflectance Spectroscopy and subdiffuse SFDI, provides new opportunities for clinical applications since they have the key advantage that they are much more sensitive to the details of the tissue scattering phase function in comparison to diffuse techniques. Since the scattering phase function is related to the subcellular structure of tissue, subdiffuse measurements have the potential to provide a powerful contrast between healthy and diseased tissue. In the subdiffuse regime, the interrogated tissue volumes are much smaller than in the diffuse regime. Whether a measurement falls within the diffuse or subdiffuse regime depends on tissue optical properties and the distance between the source and detector fiber for fiber-optic techniques or the projected spatial frequency for hyperspectral imaging and SFDI. Thus, the distance between source and detector fibers or the projected spatial frequency has important implications for clinical applications of reflectance spectroscopy and should be carefully selected, since it influences which tissue optical properties the technique is sensitive to and the size of the tissue volume that is interrogated. In this paper, we will review the opportunities and pitfalls in steady-state reflectance spectroscopy in the subdiffuse and the diffuse regime. The discussed opportunities can guide the choice of either the diffuse or subdiffuse regime for a clinical application, and the discussed pitfalls can ensure these are avoided to enable the development of robust diagnostic algorithms. We will first discuss the relevant basics of light-tissue interaction. Next, we will review all the tissue scattering phase functions that have been measured and investigate which scattering phase function models are representative of tissue. Subsequently, we will discuss the sensitivity of diffuse and subdiffuse techniques to tissue optical properties and we will explore the difference in the interrogation depth probed by diffuse and subdiffuse techniques.

KEYWORDS

reflectance spectroscopy, diffuse, subdiffuse, source-detector separation, spatial frequency domain imaging (SFDI), hyperspectral imaging (HSI), diffuse reflectance spectroscopy (DRS), single fiber reflectance spectroscopy

Introduction

When tissue changes from healthy to diseased, anatomical and physiological changes can occur which in turn can influence the absorption and scattering of light by the tissue. Reflectance spectroscopy techniques are sensitive to these changes and, therefore, have been investigated for many clinical applications (O'Sullivan et al., 2012; Lu and Fei, 2014; Akter et al., 2018; Gioux, Mazhar and Cuccia, 2019). For example, reflectance spectroscopy has been used to image resection margins during cancer surgery and to examine internal organs through endoscopes and biopsy needles (Fawzy et al., 2006; Stegehuis et al., 2017; Lin et al., 2018; McClatchy et al., 2018; Kho et al., 2019a; Jansen-Winkeln et al., 2019; Post et al., 2021). In steady-state reflectance spectroscopy, a broadband light source is used to illuminate tissue and after light interacts with tissue the remitted light is detected. Reflectance spectroscopy measurements can be performed either with fiber-optic or wide-field techniques. In fiber-optic techniques light is emitted and collected through fibers; in wide-field techniques, tissue is illuminated with either a uniform intensity (hyperspectral imaging, HSI) or a line pattern (spatial frequency domain imaging, SFDI (Cuccia et al., 2005)) and the reflected light is collected by a camera. In essence, HSI is equivalent to SFDI with a spatial frequency of zero.

For a long time, reflectance spectroscopy measurements have been performed with large distances between the source and detector fibers or low spatial frequencies, so diffusion theory could be used to extract tissue optical properties from these measurements. For diffusion theory to apply the distance between where photons are emitted and collected should be much larger than one transport mean free path $1/\mu_{tr}'$, where $\mu_{tr}' = \mu_a + \mu_s'$, μ_s' is the reduced scattering coefficient and μ_a the absorption coefficient). More recently, instrumentation and data analysis methods have been developed to perform measurements with shorter fiber distances (e.g. Single Fiber Reflectance Spectroscopy, SFR spectroscopy (Gamm et al., 2012)) and higher spatial frequencies (e.g. subdiffuse SFDI (Kanick et al., 2014)). When fiber distances are too short or spatial frequencies are too high for diffusion theory to apply, these measurements are in the so-called subdiffuse regime.

Scattering and absorption of light by tissue can be summarized in three optical properties: the scattering coefficient μ_s , the scattering phase function $p(\theta)$, and the absorption coefficient μ_a . The scattering coefficient describes the probability of a photon being scattered when it travels a certain distance through the tissue; the scattering phase function describes the probability of the direction in which a scattering event occurs; and the absorption coefficient describes the probability of a photon being absorbed when it travels a certain distance through tissue. The development of subdiffuse techniques provides new opportunities for clinical applications since they have the key advantage that they are much more

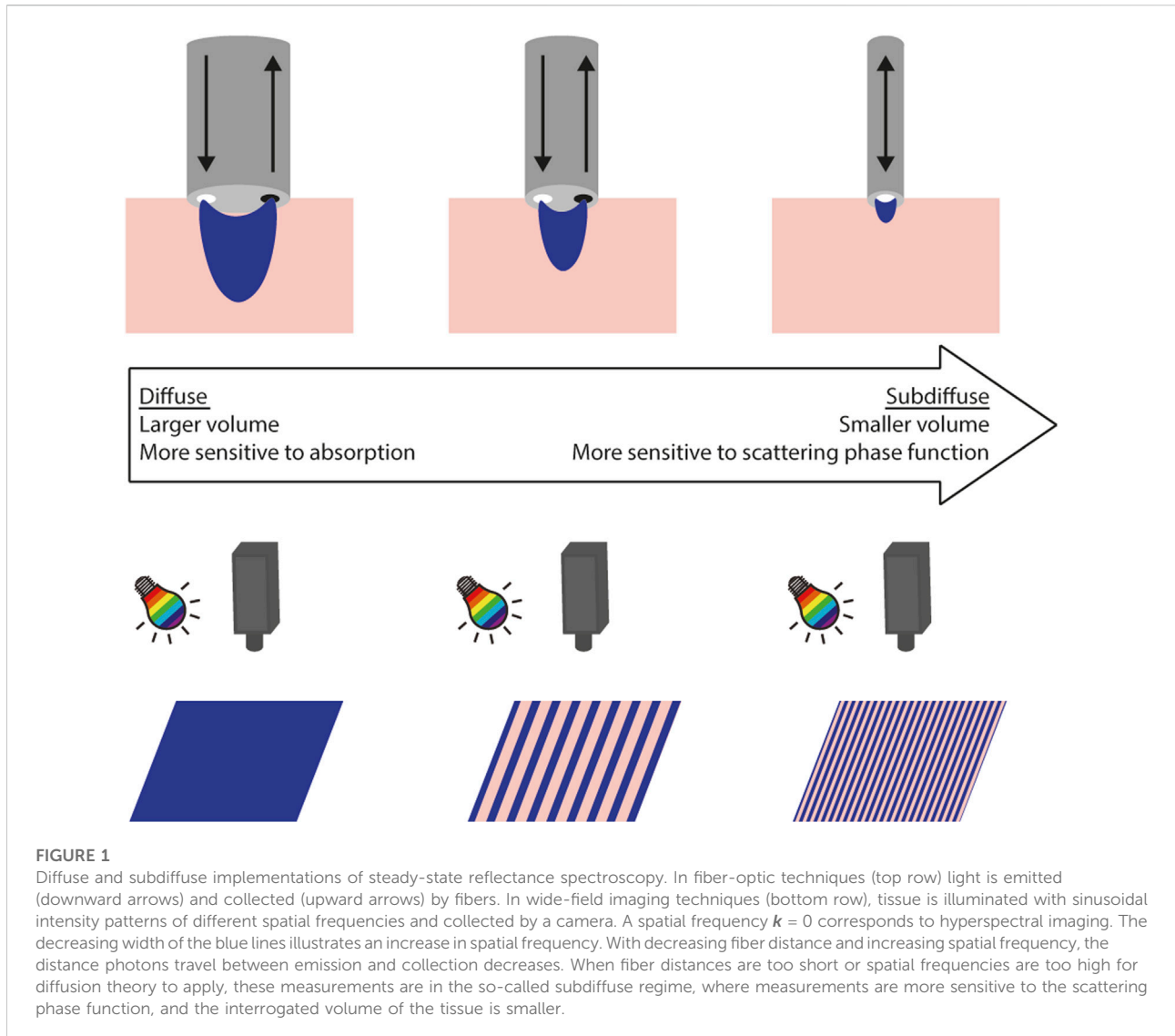
sensitive to the details of the tissue scattering phase function in comparison to diffuse techniques. Only a small number of studies have been performed where the clinical relevance of the tissue scattering phase function was investigated (either directly or with subdiffuse techniques), and the first results seem promising (Roy et al., 2009; Radosevich et al., 2013; Momi et al., 2015; Bugter and Hardillo, 2018; Bugter and Spaander, 2018; Bugter et al., 2019; Post et al., 2021). Since the scattering phase function is related to the subcellular structure of tissue, it has the potential to provide a powerful contrast between healthy and diseased tissue (Mourant et al., 1998; Drezek, Dunn and Richards-Kortum, 1999; Mourant et al., 2000). Another key difference between diffuse and subdiffuse techniques is that the interrogation volume of subdiffuse techniques is much smaller (Kanick et al., 2009; Hayakawa et al., 2018). Thus, the distance between source and detector fibers or the projected spatial frequency has important implications for clinical applications of reflectance spectroscopy, since they influence which tissue optical properties the technique is sensitive to and the size of the tissue volume that is interrogated (Figure 1).

In this manuscript, we will review the opportunities and pitfalls in steady-state reflectance spectroscopy in the subdiffuse and the diffuse regime. We will not discuss the technical details of the many different device geometries used in steady-state reflectance spectroscopy, for which we refer to the papers of (Uttinger and Richards-Kortum, 2003) for fiber-optic reflectance spectroscopy, (Lu and Fei, 2014) for hyperspectral imaging, (Gioux, Mazhar and Cuccia, 2019) for SFDI; and (O'Sullivan et al., 2012) for Diffuse Optical Imaging. The opportunities and pitfalls described in this paper generally apply to any type of reflectance spectroscopy technique. Additional opportunities and pitfalls unique to individual techniques are beyond the scope of this article.

We will first discuss the basics of light-tissue interaction relevant to understanding the difference between diffuse and subdiffuse measurements. Next, we will provide a review of all the tissue scattering phase functions that have been measured since the tissue scattering phase function is fundamental for both modeling and interpretation of subdiffuse measurements. Subsequently, we will discuss the sensitivity of diffuse and subdiffuse techniques to tissue optical properties and we will explore the difference in the interrogation depth probed by diffuse and subdiffuse techniques. Based on our review of the scattering phase function, sensitivity to optical properties, and the interrogation depth, we will discuss the opportunities and pitfalls in (sub)diffuse reflectance spectroscopy.

Monte Carlo simulations

We have performed Monte Carlo (MC) simulations to illustrate the basics of light-tissue interaction and how the sensitivity to optical properties and the interrogation depth



differs between subdiffuse and diffuse measurements. The reflectance measured with fiber-optic as well as wide-field techniques can be calculated from the reflectance as a function of radial distance $R(\rho)$ for illumination using a pencil beam. For fiber-optic measurements this entails a convolution of the pencil beam with the surface of the source fiber and integration over the surface of the detector fiber; for wide-field techniques, the Hankel Transform can be used to convert $R(\rho)$ to the reflectance as a function of spatial frequency $R(k)$ (Cuccia et al., 2009), where $k = 0$ for hyperspectral imaging. For diffusion theory to apply, photons should have scattered a large number of times before they are detected, which is generally translated into the requirement that the distance between where photons are emitted and collected should be much larger than one transport mean free path $1/\mu_{tr}'$ (Bevilacqua and Depeursinge, 1999). There is thus no clear dichotomy

between diffuse and subdiffuse measurements. Therefore, we will not perform separate analyses for diffuse and subdiffuse measurements, but we will illustrate how the sensitivity to optical properties and the interrogation depth depends on the radial distance between emission and collection of light.

For our MC simulations, we used a modified version (Post et al., 2017) of the software package MCML (Prahl, 1989; Wang, Jacques and Zheng, 1995) which enables simulating any scattering phase function using the method of (Zijp and ten Bosch, 1994). For the phase functions, we generated inverse lookup tables of 10,000 tabulated values. For each simulation we obtained histograms for the number of detected photons, the number of scattering events, the path length, the maximum depth detected photons had reached and all scattering angles of detected photons. For the reflectance, a 1D histogram was created where the weight of each detected photon was stored

TABLE 1 Phase functions used in Monte Carlo simulations. All six phase functions are Two-Term Henyey-Greenstein phase functions: $p(\theta) = \alpha \cdot p_{HG}(g_f, \theta) + (1 - \alpha) \cdot p_{HG}(g_b, \theta)$.

	g_1	p_{sb}	g_f	g_b	α
1	0.80	$4 \cdot 10^{-5}$	0.892	-0.050	0.902
2	0.80	$10 \cdot 10^{-5}$	0.930	-0.273	0.892
3	0.80	$20 \cdot 10^{-5}$	0.957	-0.393	0.883
4	0.70	$4 \cdot 10^{-5}$	0.795	-0.170	0.900
5	0.80	$4 \cdot 10^{-5}$	0.892	-0.050	0.902
6	0.90	$4 \cdot 10^{-5}$	0.950	-0.030	0.948

For each phase function the resulting scattering anisotropy g_1 and the phase function parameter p_{sb} (Post AL. et al., 2020) are given, where $p_{sb} = \frac{p_b(1^*)}{1 - p_f(23^*)} = \frac{\int_0^{2\pi} p(\theta) d\theta}{1 - \int_0^{2\pi} p(\theta) d\theta}$. Phase functions one and five are the same, but given here separately to clearly define the two sets: one with the same g_1 value, but different p_{sb} values and a second set with a single p_{sb} value and varying g_1 values

versus radial distance, with a 0.1 mm bin size. The reflectance was then normalized by dividing over the area of the annulus corresponding to that radial bin ($2\pi \cdot \rho \cdot \Delta\rho$). For the scattering angles, a 1D histogram was created where upon detection of a photon its weight was added to all the angular bins corresponding to the scattering angles it underwent. Here, 500 angular bins were used. For the number of scattering events, a 2D histogram was created where the weight, $w(N(i), \rho)$, of each detected photon was stored versus radial distance ρ with a 0.1 mm bin size and the total number of scattering events N with a bin size of 1. The average number of scattering events versus radial distance, $N_{ave}(\rho)$, was then calculated as a weighted average over the number of scattering events, $N(i)$, within each radial bin:

$$N_{ave}(\rho) = \frac{1}{\sum_{i=1}^{i=100} w(N(i), \rho)} \sum_{i=1}^{i=100} w(N(i), \rho) \cdot N(i) \quad (1)$$

For the path length and the interrogation depth, 2D histograms were created where the weight of each detected photon was stored versus radial distance with a 0.1 mm bin size and interrogation depth z (200 bins) or path length ℓ (1,000 bins) with a 0.1 mm bin size. The average interrogation depths $z_{ave}(\rho)$ and average path lengths $\ell_{ave}(\rho)$ versus radial distance were calculated as a weighted average over the interrogation depths and path lengths within each radial bin:

$$z_{ave}(\rho) = \frac{1}{\sum_{i=1}^{i=200} w(z(i), \rho)} \sum_{i=1}^{i=200} w(z(i), \rho) \cdot z(i) \quad (2)$$

and

$$\ell_{ave}(\rho) = \frac{1}{\sum_{i=1}^{i=1000} w(\ell(i), \rho)} \sum_{i=1}^{i=1000} w(\ell(i), \rho) \cdot \ell(i) \quad (3)$$

For each analysis, we will provide the optical properties of the tissue used in the MC simulations in the figure captions. Unless specified otherwise, we assumed refractive index

matching between tissue and the surrounding medium (no refraction or reflection), and photons were detected irrespective of their angle of arrival (i.e. a detection numerical aperture of 1.0). Throughout the manuscript, five different scattering phase functions have been used in MC simulations, which are specified in Table 1.

Basics of light-tissue-interaction in the diffuse and subdiffuse regime

Scattering and absorption of light by tissue can be summarized in three optical properties: the scattering coefficient μ_s ; the scattering phase function $p(\theta)$ and the absorption coefficient μ_a . The scattering coefficient describes the probability of a photon being scattered when it travels a certain distance through the tissue; the scattering phase function describes the probability of the direction in which a scattering event occurs; and the absorption coefficient describes the probability of a photon being absorbed when it travels a certain distance through tissue. The scattering coefficient and phase function are influenced by the microscopic tissue structure, while the absorption coefficient is influenced by the tissue biochemical composition (e.g. the presence of water). These three optical properties are properties of the tissue itself and vary with wavelength.

Diffusion theory is appropriate when detected photons have scattered many times. Figure 2 illustrates that close to the source diffusion theory underestimates the reflectance (Figure 2A), where photons undergo only a few scattering events and have short path lengths (Figure 2B). We compared the simulated reflectance to the model for $R(\rho)$ as proposed by (Farrell, Patterson and Wilson, 1992), which is based on diffusion theory with the Extended Boundary Condition:

$$R(\rho, \mu_s', \mu_a) = \frac{a'}{4\pi} \left[z_0 \left(\mu_{eff} + \frac{1}{r_1} \right) \frac{e^{-\mu_{eff} \cdot r_1}}{r_1^2} + (z_0 + 2z_b) \left(\mu_{eff} + \frac{1}{r_2} \right) \frac{e^{-\mu_{eff} \cdot r_2}}{r_2^2} \right] \quad (4)$$

where $a' = \mu_s' / (\mu_s' + \mu_a)$; $z_0 = 1 / (\mu_s')$; $\mu_{eff} = \sqrt{(3\mu_a\mu_s')}$; $r_1 = \sqrt{(z_0^2 + \rho^2)}$ and $r_2 = \sqrt{((z_0 + 2z_b)^2 + \rho^2)}$; $z_b = 2A / (3\mu_s')$; and A is a parameter that depends on the refractive index mismatch between the tissue and the medium above it (Martelli et al., 2009). There is no clearly defined boundary between diffuse and subdiffuse measurements, but one criterion that has been postulated for diffusion theory to apply is that photons should scatter more than approximately $4 / (1 - g_1)$ times (Faber et al., 2019), another one is that the distance between where photons are emitted and collected is more than approximately one transport mean free path $1 / \mu_{tr}'$ (Bevilacqua and Depeursinge, 1999). Also, the reduced scattering coefficient should be much larger than the absorption coefficient to ensure detected photons

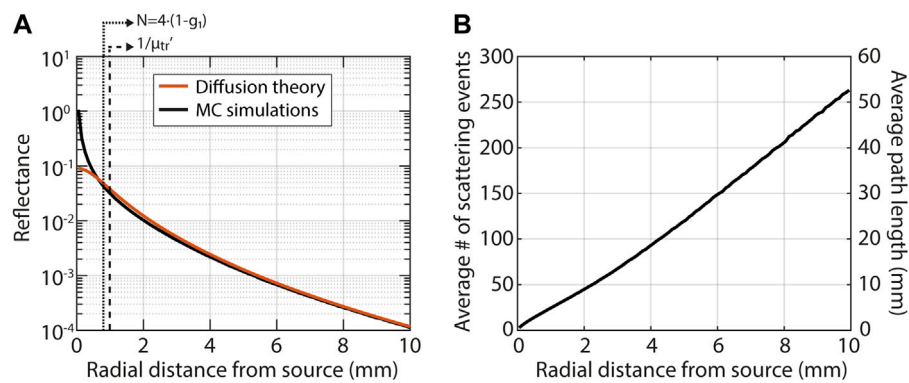


FIGURE 2

The basics of light-tissue interaction in the subdiffuse and diffuse regime illustrated with Monte Carlo simulations for a pencil beam illumination and a tissue with $\mu_s' = 1 \text{ mm}^{-1}$, $\mu_a = 0.01 \text{ mm}^{-1}$ and $g = 0.8$. There is no clearly defined boundary between diffuse and subdiffuse measurements, two criteria that have been proposed are indicated by the dashed lines in the left figure. (A) Diffusion theory (Eq. 4) severely underestimates the reflectance close to the source, in the so-called subdiffuse regime. (B) In the subdiffuse regime detected photons underwent few scattering events (left axis) and traveled short path lengths (right axis).

have scattered many times. For the optical properties used in the simulations for Figure 2, that would translate to photons traveling a radial distance of at least 0.99 mm or scattering at least 20 times (which occurs at a radial distance of 0.78 mm), which is within the region where diffusion theory deviates from the simulated reflectance.

Scattering phase function

A key difference between reflectance in the diffuse and subdiffuse regime is the influence of the scattering phase function (Mourant et al., 1996; Bevilacqua and Depeursinge, 1999; Calabro and Bigio, 2014). In the subdiffuse regime, photons have scattered only a few times before they are detected and, therefore, the scattering phase function greatly influences the measured reflectance. In the diffuse regime, photons have scattered many times before they are detected and, therefore, the effect of the scattering phase function is much less. In 2014, Calabro and Bigio published a review on the influence of the tissue scattering phase function in reflectance spectroscopy, demonstrating the importance of properly incorporating the influence of the scattering phase function for short source-detector separations and stating that the importance of the scattering phase function was chronically overlooked (Calabro and Bigio, 2014). Since then, more research has been done on incorporating the influence of the scattering phase function into forward models, which we will discuss here. Even so, often enough the influence of the scattering phase function is still not properly taken into account when analyzing subdiffuse reflectance spectroscopy measurements.

No analytical model exists that describes the reflectance for the entire range from subdiffuse to diffuse measurements. For the diffuse regime, analytical models exist to derive optical properties from the measured reflectance, but these do not exist in the subdiffuse regime. Some analytical models exist to describe light-tissue interaction in the subdiffuse regime, but their application has been limited (Vitkin et al., 2011; Xu, 2016; Piao and Patel, 2017). In the subdiffuse regime, semi-empirical models exist for some specific device geometries (such as the model for SFR Spectroscopy (Post A. L. et al., 2020)) which are based on MC simulations. For device geometries where no models exist, optical properties are extracted based on look-up-tables or machine-learning algorithms—both also based on MC simulations (Hennessy et al., 2013; Vervandier and Gioux, 2013; Chen et al., 2016; Ivančič et al., 2018; Stier et al., 2021; Erickson, Durkin and Tunnell, 2022). It is thus imperative to understand which phase function models accurately represent tissue scattering phase functions since any optical property extraction in the subdiffuse regime is thus directly or indirectly based on MC simulations. Therefore, we have performed a literature review of measured tissue scattering phase functions and identified which scattering phase function models are representative of tissue.

In general, Mie theory can be used to calculate the scattering phase function for a single spherical particle with a given radius and refractive index. One approach to model the tissue scattering phase function is using Mie theory for a fractal size distribution of scattering particles (Wang, 2000). The phase function for the size distribution is then calculated as:

$$p_{Mie}(\theta) = \frac{\sum_{i=1}^n \sigma_s(\theta; r_i) n(r_i)}{\sum_{i=1}^n \sigma_s(r_i) n(r_i)} = \frac{\sum_{i=1}^n p(\theta; r_i) \sigma_s(r_i) n(r_i)}{\sum_{i=1}^n \sigma_s(r_i) n(r_i)} \quad (5)$$

TABLE 2 Overview of phase function models that provided the best fit (last column) to measured phase functions.

Paper	Tissue type	Angles	PF in publication	PF best fit
Mourant et al. (1998)	Cells	2–171	HG	Mie
Xu, Wu and Qu, (2008)	Cells	1.1–165	Mie size distribution	MHG
Hammer, Yaroslavsky and Schweitzer, (2001)	Blood	2.5–175	RMC	MPC
Yaroslavsky et al. (1996)	Blood	0–160	RMC	MPC
van der Zee, Essenpreis and Delpy, (1993)	Gray Matter	0–170	-	TTHG
van der Zee, Essenpreis and Delpy, (1993)	White Matter	0–170	-	TTHG
Saccomandi et al. (2015)	Muscle	0–141	TTHG	TTHG
Zijp and ten Bosch, (1998)	Muscle (Bovine)	0–179 ^a	TTHG	TTHG
Firbank et al. (1993)	Skull	2–160	-	RMC
Ghosh et al. (2001)	Malignant Breast	10–165	TTHG and HG	TTHG
Ghosh et al. (2001)	Healthy Breast	10–165	TTHG and HG	TTHG
Marchesini et al. (1989)	Liver	5–150	TTHG	TTHG
Saccomandi et al. (2015)	Liver	0–141	TTHG	TTHG
Saccomandi et al. (2015)	Pancreas	0–141	TTHG	TTHG
Marchesini et al. (1989)	Lung	5–150	TTHG	TTHG
Marchesini et al. (1989)	Uterus	5–150	TTHG	MHG
Forster et al. (2006)	Dentin (parallel)	0–172	-	RMC
Forster et al. (2006)	Dentin (perpendicular)	0–172	-	MHG
Arnfield, Tulip and Mcphee, (1988)	Rat Tumor	0–165	-	TTHG
Taddeucci et al. (1996)	White Matter (Bovine)	0–3	Mie Theory	-
Taddeucci et al. (1996)	Gray Matter (Bovine)	0–3	Mie Theory	-
Gareau, (2006)	Skin (Murine)	1–12	HG	-
Yaroslavskaya et al. (1994)	Epidermis	3–25	HG	-
Okamoto Ugnell and Öberg, (1997)	Bone (Guinea Pig)	-50-50	HG	-
Jacques et al. (1987)	Dermis (20 µm thick)	-50-50	HG	-
Jacques et al. (1987)	Dermis (280 µm thick)	-50-50	MHG	-
Bruls and Van Der Leun, (1984)	Epidermis	-60-60	-	-
Bruls and Van Der Leun, (1984)	Stratum Corneum	-60-60	-	-
Wietlicka-piszcz, Mazur and Grzegorzewski, (1994)	Skull bones	-90-90	-	-

A literature review of measured tissue scattering phase functions resulted in 29 measurements. For measurements that included backward scattering ($>90^\circ$), we extracted the measured phase function data and performed fits with six phase function models (Mie, HG, MHG, TTHG, RMC, MPC) to identify the model with the lowest (τ RSE). For each measured phase function the angular range over which the measurement was performed is given; which model was used in the corresponding manuscript to describe the measured phase function; and which model resulted in the lowest (τ RSE). Mie = Mie theory for a fractal size distribution, HG = Henyey-Greenstein; MHG = Modified Henyey-Greenstein; TTHG = Two-Term Henyey-Greenstein; RMC = Reynolds McCormick; MPC = Modified Power of Cosines.

^aFor Zijp et al. the angles from 74 to 132 were excluded from the fit, since the authors indicated their measurements underestimated the phase function at those angles due to shading by the sample holder.

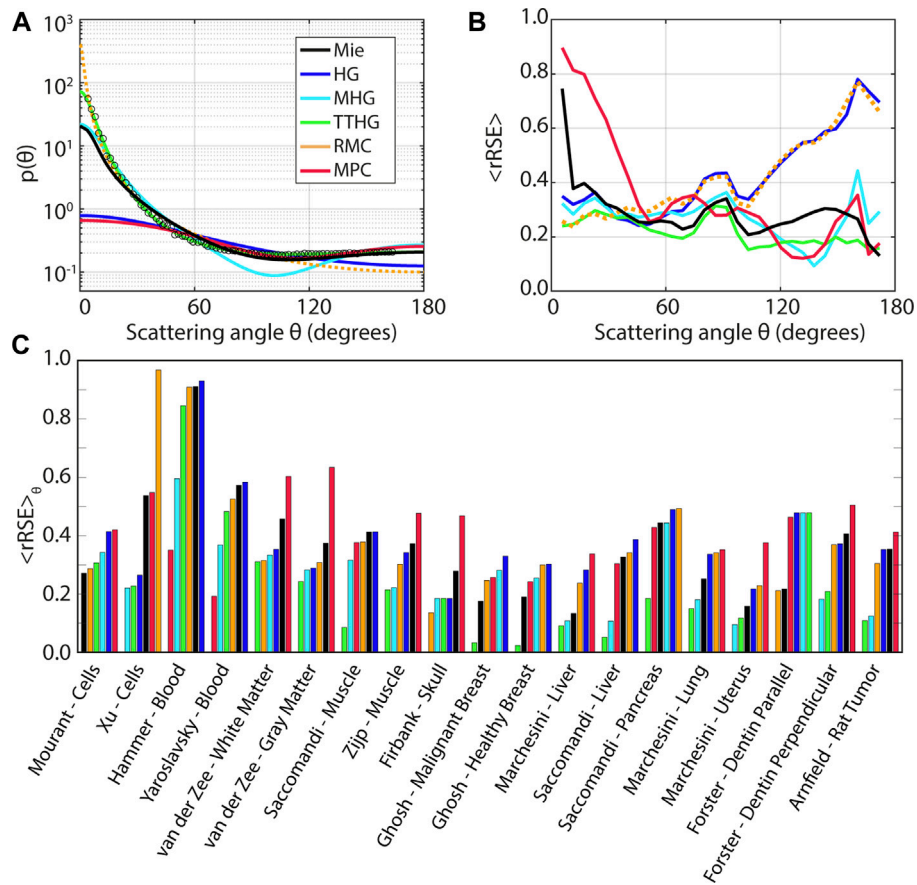


FIGURE 3

Six phase function models have been proposed for tissue: Mie for a fractal size distribution (Mie), Henyey-Greenstein (HG); Modified Henyey-Greenstein (MHG), Two-Term Henyey-Greenstein (TTHG), Reynolds McCormick (RMC), and Modified Power of Cosines (MPC). A literature review of measured tissue scattering phase functions resulted in 29 measurements, for which we performed fits with each model and identified the model with the lowest average relative root-square-error $\langle rRSE \rangle$. Ten phase functions were excluded from the analysis since they only measured the phase function in the forward direction (A) Example of a phase function measured by (Ghosh et al., 2001) of healthy breast tissue and the fit results, where the TTHG provides the best description of the data. (B) Average $rRSE$ versus scattering angle for all 19 phase functions for which we performed a fit. On average, the TTHG has the lowest $\langle rRSE \rangle$ over the full angular range, followed by the MHG. The HG and RMC cannot accurately capture backward scattering angles, and Mie for a fractal size distribution and the MPC cannot accurately capture forward scattering angles. (C) For the majority of measurements (11) the TTHG was the best fit, followed by the MHG (3), RMC (2), MPC (2) and Mie for a fractal size distribution (1). The HG was never the best model and performed poorly overall.

where σ_s is the differential cross section and $n(r_i)$ is the number of particles with radius r_i , and the size distribution of particles is described by:

$$n(r_i) = (d_i)^{-\alpha} = (2r_i)^{-\alpha} \quad (6)$$

where α is the fractal dimension and d_i the particle diameter.

Other scattering phase function models use simple analytic expressions. One of the first such models that was proposed for tissue was the Henyey-Greenstein (HG) phase function:

$$p_{HG}(\mu, g_{HG}) = \frac{1}{4\pi} \frac{1 - g_{HG}^2}{(1 + g_{HG}^2 - 2g_{HG}\mu)^{3/2}} \quad (7)$$

where $\mu = \cos(\theta)$ and θ is the scattering angle. For the HG phase function, the scattering anisotropy g_1 is equal to g_{HG} . The HG was proposed to approximate Mie theory. The HG phase function provides accurate results in simulations of diffuse measurements. However, the HG phase function underestimates backscattering. Subdiffuse measurements are particularly sensitive to small angle backscattering events (Canpolat and Mourant, 2000; Post AL. et al., 2020) and, therefore, the HG phase function is not appropriate to model subdiffuse measurements. To account for backscattering, the modified Henyey-Greenstein (MHG) was proposed (Jacques et al., 1987), which adds an isotropic term to the HG, as well as the two-term Henyey Greenstein (Pfeiffer and Chapman,

2008) (TTHG, also known as double HG) which is the sum of two HG phase functions, one with forward directed scattering and one with backward directed scattering:

$$p_{MHG}(\mu, \alpha, g_{HG}) = \alpha p_{HG}(\mu) + (1 - \alpha) \frac{3}{4\pi} \mu^2 \quad (8)$$

$$p_{TTHG}(\mu, \alpha, g_f, g_b) = \alpha p_{HG}(\mu, g_f) + (1 - \alpha) p_{HG}(\mu, g_b) \quad (9)$$

For both the MHG and the TTHG α lies between 0 and 1. For the TTHG, g_f parametrizes scattering in the forward direction and lies between 0 and 1, while g_b parameterizes scattering in the backward direction and lies between -1 and 0. Two other scattering phase functions that have been proposed for tissue are the Reynolds McCormick (RMC, also known as Gegenbauer kernel) (Reynolds and McCormick, 1980) and the modified power of cosines (Bevilacqua and Depeursinge, 1999) (MPC):

$$p_{RMC}(\mu, \alpha, g_{RMC}) = K (1 + g_{RMC}^2 - 2g_{RMC}\mu)^{-(\alpha+1)} \quad (10)$$

where

$$K = \pi^{-1} \alpha g_{RMC} (1 - g_{RMC}^2)^{2\alpha} [(1 + g_{RMC})^{2\alpha} - (1 - g_{RMC})^{2\alpha}]^{-1} \quad (11)$$

and

$$p_{MPC}(\mu, \alpha, N) = \alpha p_{PC} + (1 - \alpha) \left(\frac{3}{4\pi}\right) \mu^2 \quad (12)$$

where

$$p_{PC} = \frac{1}{4\pi} \frac{N+1}{2^N} (1 + \mu)^N \quad (13)$$

From our literature search, we identified 19 papers in which 29 scattering phase functions had been measured (Table 2). In some papers no fit was performed with a scattering phase function model, in other papers a fit with only one type of scattering phase function seemed to have been performed. To investigate which scattering phase function models best represent the tissue scattering phase function, we extracted the measured phase functions from the papers and performed fits with all six phase function models (Mie, HG, MHG, TTHG, RMC, and MPC). The goal was not to identify a single phase function model that would be representative for any tissue type, but to identify which phase function models best represent measured tissue scattering phase functions.

Since the main difference between the phase function models is in the backward scattering direction, ten measured phase functions were excluded from the analysis since they only measured in the forward direction ($<90^\circ$, last rows of Table 2). For the remaining 19 phase functions, the phase function model that resulted in the best fit based on the average relative error between the fit and the data is given in the last column of Table 2. The Mie phase function for a fractal

size distribution was the best fit for one measured scattering phase function, the HG was never the best model, the TTHG in 11 measurements, MHG in 3, RMC in 2, and MPC in 2.

An example of a fit is shown in Figure 3A for the phase function of healthy breast tissue as measured by (Ghosh et al., 2001). The TTHG is the best fit to the measured data; the MPC and HG are the worst. The RMC underestimates the backscattering and the MHG and Mie for a fractal size distribution underestimate forward scattering. In Figure 3B the average relative root squared error $\langle rRSE \rangle$ is shown versus scattering angle for all phase functions, per phase function model, where:

$$rRSE(\theta) = \frac{\sqrt{(p_{fit}(\theta) - p(\theta))^2}}{p(\theta)} \quad (14)$$

and the average of the rRSE, $\langle rRSE \rangle$, is calculated for each angle over all the measured phase functions. In general, the MHG and the TTHG result in the lowest errors over the full angular range, followed by Mie theory for a fractal size distribution. The RMC and the HG are inaccurate in the backward scattering direction. Mie for a fractal size distribution and the MPC underestimate scattering in the forward direction. In Figure 3C the rRSE averaged over all angles and all measured scattering phase functions, $\langle rRSE_\theta \rangle$ of the fit results for all the scattering phase functions in Table 2 are given.

The scattering phase function can be represented by a series of i Legendre polynomials, weighted by their moments g_i . The first moment, g_1 is known as the scattering anisotropy. In the diffuse regime, the influence of the scattering phase function can be captured by the parameter g_1 , the scattering anisotropy, which is equal to the average value of the cosine of the scattering angle: $g_1 = \langle \cos \theta \rangle$. For high values of g_1 , scattering events will be mostly forward directed, for lower values of g_1 scattering will be more isotropic. In diffusion theory models, the scattering coefficient μ_s and the scattering anisotropy g_1 are combined in a single parameter, the reduced scattering coefficient μ_s' . For different combinations of μ_s and g_1 , but the same value of μ_s' , the measured reflectance will be the same. In the subdiffuse regime, g_1 is not sufficient to capture the influence of the scattering phase function (Bevilacqua and Depeursinge, 1999; Bodenschatz et al., 2016; Naglič et al., 2017; Post AL. et al., 2020). Several parameters have been proposed to capture the scattering phase function influence in the subdiffuse regime: γ (Bevilacqua and Depeursinge, 1999), δ (Tian, Liu and Wang, 2006; Naglič et al., 2016), σ (Bodenschatz et al., 2016), R_{pNA} (Post et al., 2017) and p_{sb} (Post AL. et al., 2020). The parameters γ , δ and σ all incorporate the Legendre moments g_n of the tissue scattering phase function. $\gamma = (1 - g_2)/(1 - g_1)$; $\delta = (1 - g_3)/(1 - g_1)$; and $\sigma = \sum_{i=2}^{\infty} (-0.5)^{i-2} (1 - g_i)/(1 - g_1)$. The parameters R_{pNA} and p_{sb} are based on the assumption that detected photons undergo an arbitrary number of forward events

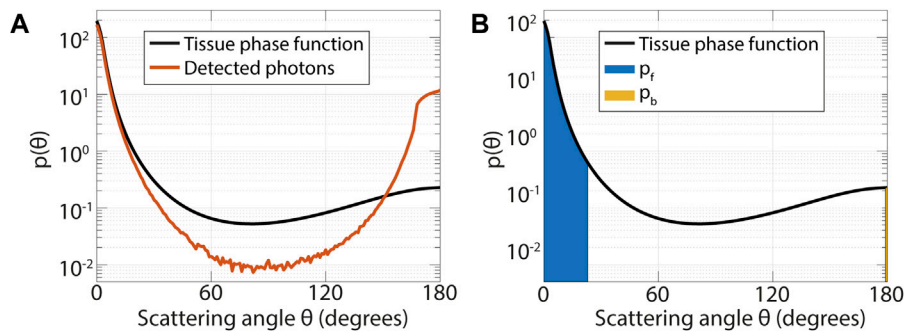


FIGURE 4

(A) In the subdiffuse regime detected photons mainly undergo scattering events at small angles in the forward and backward direction. Results from a Monte Carlo simulation with a pencil beam illumination and detection over a radial distance from 0 to 0.1 mm from the source with a numerical aperture of 0.22, for a tissue with $\mu_s' = 1 \text{ mm}^{-1}$, $\mu_a = 0.01 \text{ mm}^{-1}$; $g = 0.8$; $p_{sb} = 4 \cdot 10^{-5}$ and a refractive index of 1.35. (B) The phase function parameter p_{sb} incorporates the probability of scattering at small angles, where p_{sb} is equal to the probability of backward scattering within 1° (p_b , yellow area) divided by one minus the probability of forward scattering within 23° (p_f , blue area). The probability of scattering within a certain angle is equal to the integral of the phase function over the angular range (shaded areas).

in combination with a single backscattering event. In that case, the probability of detection of a photon would be equal to:

$$R_p = \frac{p_b}{1 - p_f} = \frac{2\pi \int_{\pi-\theta_b}^{\pi} p(\theta) \sin\theta d\theta}{1 - 2\pi \int_0^{\theta_f} p(\theta) \sin\theta d\theta} \quad (15)$$

where p_b is the probability of backward scattering and p_f the probability of forward scattering. R_{pNA} is based on the assumption that only photons that scatter at angles smaller than or equal to the acceptance angle of the fiber are detected. In that case the probabilities of forward and backward scattering, p_b and p_f , are equal to the integrals of the scattering phase function over the acceptance angle in the backward and forward direction, respectively. The acceptance angle is related to the numerical aperture (NA) of a system, which explains the name of R_{pNA} . The same group later developed the parameter p_{sb} , which uses an integration angle of 1° in the backward direction and 23° in the forward direction (Post AL. et al., 2020). The details of the derivation of R_{pNA} and p_{sb} can be found in (Post et al., 2017) and (Post AL. et al., 2020), respectively. For all 5 phase function parameters, the exact relation between their values and the tissue composition is not known.

Figure 4A shows results from an MC simulation for a pencil beam illumination and detection within the first 100 μm from the source with a numerical aperture of 0.22. The black line is the tissue scattering phase function that was used in the simulation, the red line is the histogram of scattering angles of detected photons (the effective phase function (Post AL. et al., 2020)). Figure 4A illustrates that detected photons mostly undergo scattering events at small angles in the forward and backward directions. The sensitivity of subdiffuse measurements to small-angle backscattering events has also been shown by (Canpolat and Mourant, 2000). For SFR spectroscopy, the subdiffuse limit

for fiber-optic measurements (since the source and detector fiber overlap), it has been shown that p_{sb} is most appropriate to model the reflectance (Post AL. et al., 2020). The parameter p_{sb} is equal to (Figure 4B):

$$p_{sb} = \frac{p_b(1^\circ)}{1 - p_f(23^\circ)} = \frac{\int_{179}^{180} p(\theta) d\theta}{1 - \int_0^{23} p(\theta) d\theta} \quad (16)$$

where p_b is the probability of backward scattering within 1° , which is equal to the integral of the scattering phase function over $179\text{--}180^\circ$, and p_f is the probability of forward scattering within 23° , which is equal to the integral of the scattering phase function over $0\text{--}23^\circ$.

The parameter p_{sb} was specifically developed for SFR Spectroscopy, where the source and detector fiber overlap. Here, we show that the parameter p_{sb} can also be used to accurately describe the reflectance at larger radial distances from the source. In Figure 5 the influence of the scattering phase function on the measured reflectance is illustrated for two sets of TTHG phase functions. One set where g_1 was the same for all three phase functions but p_{sb} varied (phase functions 1–3, Table 1); one set where p_{sb} was the same for all three phase functions, but g_1 varied (phase functions 4–6, Table 1). These phase functions were selected by calculating g_1 and p_{sb} values for a large number of TTHG phase functions with a wide range of parameters. It should be noted that multiple TTHG phase functions could have the same g_1 and p_{sb} values, therefore, we give the specific parameters in Table 1.

Figure 5A shows that g_1 does not capture the scattering phase function influence properly close to the source, since different phase functions with the same g_1 value (and different p_{sb} values) result in a different reflectance close to the source. Further away

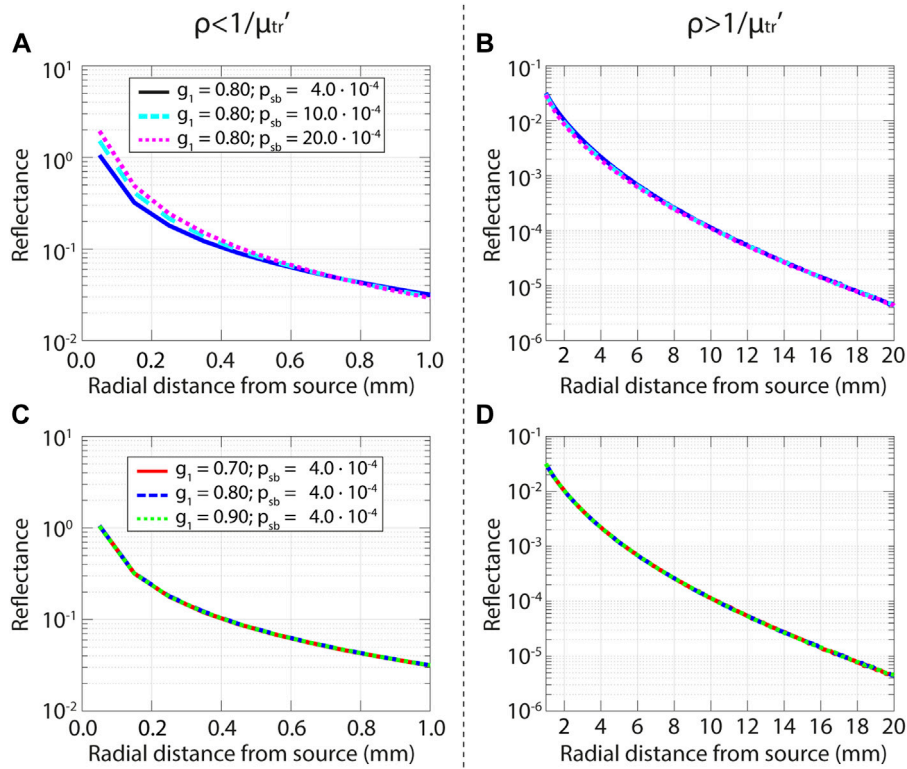


FIGURE 5

Influence of the phase function on the reflectance as a function of radial distance from the source for the subdiffuse regime (left, up to $1/\mu_{tr}'$) and the diffuse regime (right, from $1/\mu_{tr}'$). Results from Monte Carlo simulations with a pencil beam illumination for a tissue with $\mu_s' = 1.0 \text{ mm}^{-1}$, $\mu_a = 0.01 \text{ mm}^{-1}$. (A) Reflectance for three different phase functions, with the same g_1 value, but different p_{sb} values. Close to the source the reflectance values do not overlap, indicating that g_1 does not accurately capture the influence of the phase function. (C) Reflectance for three different phase functions with the same p_{sb} value, but different g_1 values. Close to the source, the reflectance values overlap, indicating that p_{sb} does capture the influence of the phase function in the subdiffuse regime. (B,D) In the diffuse regime, the details of the tissue scattering phase function do not influence the measured reflectance anymore and is only a function of μ_s' and μ_a . Since p_{sb} also captures the phase function influence further away from the source, this suggests that p_{sb} is not only suitable for SFR spectroscopy, but for the entire subdiffuse to diffuse regime.

from the source (Figure 5B), the difference in reflectance values between the three phase functions is much smaller. Figure 5C illustrates that p_{sb} does capture the scattering phase function influence properly close to the source; phase functions with the same p_{sb} values, but different g_1 values result in the same reflectance. Figure 5D shows that p_{sb} also captures the scattering phase function influence further away from the source, suggesting that p_{sb} is not only suitable for SFR spectroscopy, but for the entire subdiffuse to diffuse regime.

Sensitivity to optical properties

Diffuse and subdiffuse measurements have different sensitivities to optical properties, which is illustrated in

Figure 6. In the diffuse regime, measurements are more sensitive to the absorption coefficient, while in the subdiffuse regime measurements are more sensitive to both the reduced scattering coefficient and p_{sb} . In Figure 6 for each subplot one optical property is varied, and the relative differences in reflectance values are calculated with respect to the lowest optical property (ΔR). For example, for the first set, we varied the absorption coefficient $\mu_a = [0.1 \ 0.3 \ 0.5] \text{ mm}^{-1}$, while keeping the other optical properties constant, and we determined the relative difference between the reflectance for $\mu_a = 0.3 \text{ mm}^{-1}$ and for $\mu_a = 0.5 \text{ mm}^{-1}$ compared to the simulations with $\mu_a = 0.1 \text{ mm}^{-1}$. Thus for $\mu_a = 0.3 \text{ mm}^{-1}$ ΔR is equal to:

$$\Delta R = \left| \frac{R_{\mu_a=0.3} - R_{\mu_a=0.1}}{R_{\mu_a=0.1}} \right| \cdot 100\% \quad (17)$$

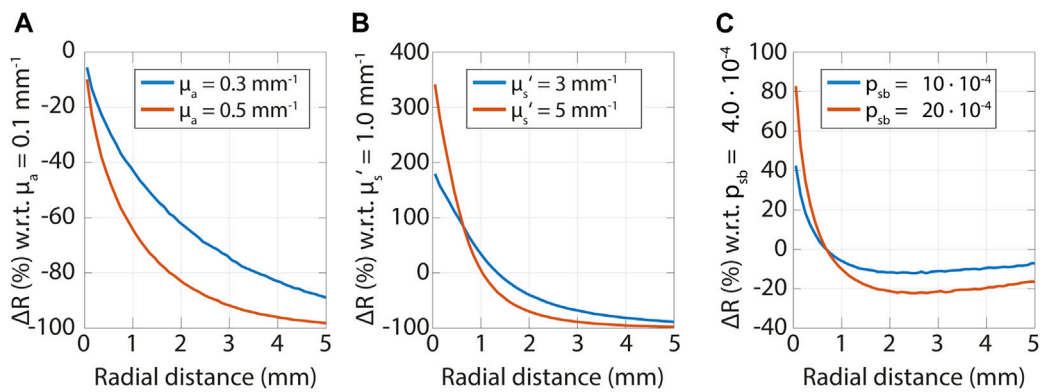


FIGURE 6 Sensitivity to tissue optical properties versus radial distance. In each subfigure, the relative change in the reflectance is shown as a function of radial distances for changes in an optical property. Note that the sensitivity is related to the absolute value of ΔR . In the subdiffuse regime, measurements are more sensitive to both the reduced scattering coefficient and p_{sb} , while in the diffuse regime measurements are more sensitive to the absorption coefficient. **(A)** Change in the reflectance for two values of the absorption coefficient (0.3 and 0.5 mm^{-1}) relative to the reflectance for an absorption coefficient of 0.1 mm^{-1} . **(B)** Change in the reflectance for two values of the reduced scattering coefficient (3 and 5 mm^{-1}) relative to the reflectance for a reduced scattering coefficient of 1 mm^{-1} . **(C)** Change in the reflectance for two values of p_{sb} ($10 \cdot 10^{-5}$ and $20 \cdot 10^{-5}$) relative to the reflectance for a p_{sb} of $4 \cdot 10^{-4}$.

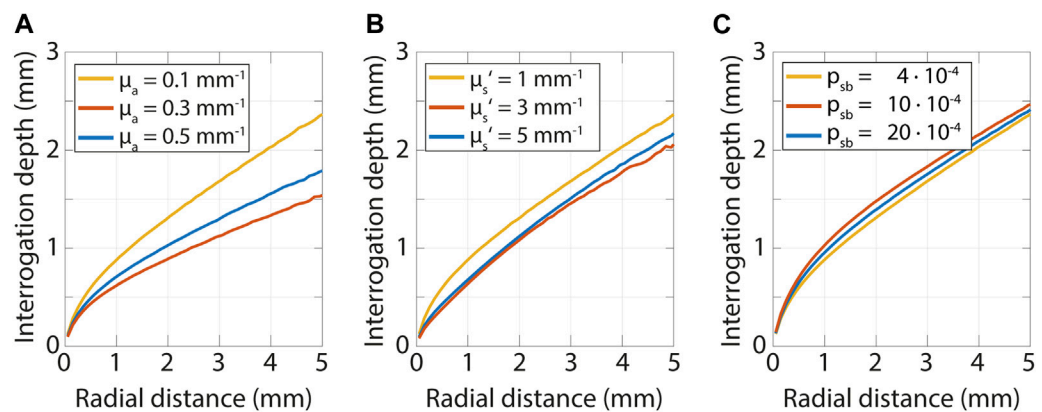


FIGURE 7 Interrogation depth versus radial distance from a pencil beam source obtained from Monte Carlo simulations while varying the absorption coefficient, scattering coefficient and p_{sb} . The interrogation depth mainly depends on the radial distance from the source and the absorption coefficient of the tissue. **(A)** Variation of absorption coefficient while $\mu_s' = 1.0 \text{ mm}^{-1}$ and $p_{sb} = 4 \cdot 10^{-5}$. **(B)** Variation of scattering coefficient while $\mu_a = 0.1 \text{ mm}^{-1}$ and $p_{sb} = 4 \cdot 10^{-5}$. **(C)** Variation of p_{sb} while $\mu_s' = 1.0 \text{ mm}^{-1}$ and $\mu_a = 0.1 \text{ mm}^{-1}$.

These sensitivities can be related to Figure 2, where we showed that photons that are detected close to where they were emitted underwent only a few scattering events and traveled short path lengths. The absorption attenuates the reflectance by a factor of $e^{-\mu_a \ell}$, where ℓ is the path length in the absence of absorption. Thus, further away from the source where photons have traveled longer paths the influence of the absorption is much more. Since photons that are detected close to the source have only scattered a few times, the direction is not randomized and the details of the scattering phase function strongly influence the measured reflectance. Therefore, close

to the source measurements are more sensitive to the scattering phase function and thus to p_{sb} .

Interrogation depth

The depth detected photons have reached in the tissue depends on both the tissue optical properties and the distance between the source and detector. This relation is illustrated in Figure 7, where the interrogation depth is shown for a range of optical properties and distances between emission and detection

of photons. The interrogation depth is defined here as the average depth detected photons have traveled. We varied the absorption coefficient, reduced scattering coefficient, and p_{sb} , to show their effects on the interrogation depth.

The interrogation depth is mainly influenced by the source-detector-separation and the absorption coefficient of the tissue. The reduced scattering coefficient and p_{sb} have a smaller influence. The influence of the scattering anisotropy is not shown here but has been found to also have a minor influence on the interrogation depth (Kanick et al., 2009; Hennessy et al., 2014). Methods and models to determine the interrogation depth for a specific measurement geometry can be found for SFDI in (Bodenschatz et al., 2015) and (Hayakawa et al., 2018), and for fiber-optic spectroscopy in (Kanick et al., 2009) and (Hennessy et al., 2014).

Discussion

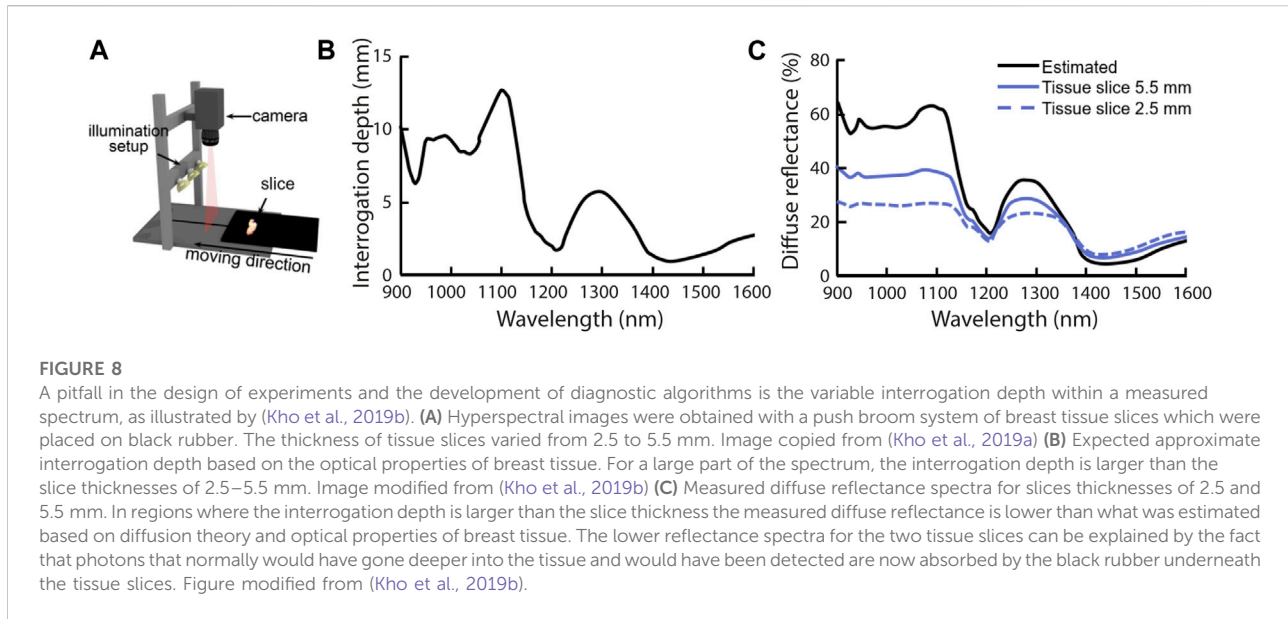
Whether measurements are in the diffuse or subdiffuse regime is influenced by the tissue optical properties and the distance between source and detector fibers or the projected spatial frequency. There is no clear dichotomy between the diffuse and subdiffuse regime, but measurements are in the diffuse regime when the distance between source and detector fibers is large or the projected spatial frequency is low compared to the transport mean free path of the tissue. When measurements cannot be described by diffusion theory they are in the so-called subdiffuse regime. In the diffuse regime, the reflectance can be described as a function of the absorption and reduced scattering coefficient. For smaller distances, details in the scattering phase function have to be taken into account as well. Since the scattering phase function is related to the subcellular structure of tissue, subdiffuse measurements have the potential to provide a powerful contrast between healthy and diseased tissue.

Since the fiber distance or spatial frequency influences which tissue optical properties the reflectance method is sensitive to and the size of the tissue volume that is interrogated, the choice for a certain distance or frequency has important implications for clinical applications of reflectance spectroscopy. Often enough, the fiber distance or spatial frequency used in a clinical study is based on practical considerations such as the availability of a probe with fixed fiber distances. Based on our review, we want to encourage researchers to carefully select the fiber distance or spatial frequency for a clinical application, since it has important consequences for its ability to answer a clinical question. Also, we would implore researchers to always supply the reasoning behind the fiber distance or spatial frequency in the methods section of a manuscript. When the interrogation depth is essential to the clinical application, this should drive the choice for a fiber distance or spatial frequency. For

example, for margin assessment in breast cancer, the surgeon wants to know whether there is tumor tissue within the first 2 mm from the tissue surface. When the interrogation depth is not essential for a clinical application, the sensitivity to optical properties should drive the choice for a fiber distance or spatial frequency.

Sensitivity to optical properties

Subdiffuse measurements have the key advantage that they are much more sensitive to the tissue scattering phase function compared to diffuse techniques, more specifically to scattering at small angles in the forward and backward direction (Canpolat and Mourant, 2000; Post AL. et al., 2020; Stewart et al., 2020). The phase function is related to the subcellular structure of tissue. The exact relationship between the subcellular structure of tissue and different scattering phase function models and parameters used in these scattering phase function models is not well-known. The volume fraction of organelles influences the total amount of scattered light as well as the angular distribution of scattered light (Drezek, Dunn and Richards-Kortum, 1999). (Mourant et al., 1998) and (Drezek, Dunn and Richards-Kortum, 1999) showed that mitochondria and other organelles with similar sizes (in the order of a micron) result in scattering at small angles in the forward direction, while nuclei are related to small angle scattering in the forward direction. Another study suggests that scattering at angles greater than approximately 110° is correlated with the DNA content of cells (Mourant et al., 2000). The full clinical potential of the characterization of the scattering phase function has not yet been explored, but a small number of studies with subdiffuse techniques have shown promising results (McClatchy et al., 2016; Bugter and Hardillo, 2018; Bugter and Spaander, 2018; Bugter et al., 2019; Post et al., 2021; Streeter et al., 2021). For example, Post et al. have shown that SFR spectroscopy could discriminate between non-dysplastic Barrett's mucosa and neoplasia with an area under the curve of 0.94 based on scattering properties of tissue alone (the scattering amplitude, scattering slope, and p_{sb} at 500 nm) (Post et al., 2021). Even more interesting, sensitivity to the tissue scattering phase function might enable detecting changes in tissue that are not (yet) visible by eye since the tissue scattering phase function is related to the subcellular structure of tissue. For example, before the development of a tumor, cell lineages can acquire pro-tumorigenic genetic mutations, which can grow in large areas of cells that are predisposed to progress to a malignant lesion—an effect known as field cancerization. These areas of cells can have acquired some, but not all phenotypic changes related to malignancy (Curtius, Wright and Graham, 2017). A small number of studies with subdiffuse reflectance spectroscopy have shown promise for the detection of field cancerization, e.g. with SFR spectroscopy for esophageal cancer (Bugter and Spaander, 2018; Post et al., 2021). Other



subdiffuse techniques such as enhanced backscatter spectroscopy have also shown promise for the detection of field cancerization in colon cancer (Roy et al., 2009).

Diffuse reflectance measurements are more sensitive to the absorption coefficient. However, this does not necessarily mean diffuse measurements are the best choice when absorption properties are related to the disease state of tissue. If the tissue has a high absorption coefficient, the measured reflectance values might become so low that there is almost no signal regardless of the concentration of the absorber (e.g. blood) and subdiffuse techniques should be used instead.

Whenever the interrogation depth is less important, we would recommend performing a pilot study to identify the optimal fiber distance or spatial frequency that provides maximum contrast between tissue types. For any fiber-optic probe, one could always include an SFR measurement by also illuminating and collecting through one fiber. Furthermore, probes could be used with multiple fiber distances (Lin et al., 1997). Since it is very easy to perform measurements with multiple spatial frequencies for wide-field imaging techniques, we would recommend always investigating which spatial frequencies provide the best clinical results.

Interrogation depth

For clinical applications where the interrogation depth is critical, an important opportunity in reflectance spectroscopy is the ability to choose the fiber distance or spatial frequency to obtain the required interrogation depth. However, since the absorption coefficient has a major influence on the

interrogation depth and the absorption coefficient can vary by a few orders of magnitude within a spectrum, the interrogation depth will vary significantly with wavelength for a constant fiber distance or spatial frequency. The issue of variable penetration depth should be considered when designing experiments and developing diagnostic algorithms. A study by Kho et al. illustrates this pitfall for hyperspectral imaging (Kho et al., 2019b). They performed measurements with a pushbroom hyperspectral imaging setup on slices of resected breast tissue, where the tissue was placed on black rubber (Figure 8A). The thickness of the tissue slices varied from 2.5 to 5.5 mm. Figure 8B shows the estimated interrogation depth for adipose tissue (90% fat, 10% water) and Figure 8C shows the estimated diffuse reflectance for adipose tissue (black solid line), and the average measured spectrum for a tissue slice of 5.5 mm thick (blue solid line) and for a tissue slice of 2.5 mm thick (blue dashed line). The difference between the spectra for different slice thicknesses underlines the importance of knowing the interrogation depth for the device geometry used and the tissue that is interrogated. Because the tissue slices are thinner than the interrogation depth at some wavelengths, the thickness itself will influence the measured reflectance. Photons that normally would have gone deeper into the tissue and would have been detected are now absorbed by the black rubber underneath the tissue slices. If a diffusion theory model would be used to fit the measured spectra this would result in inaccurate retrieved optical properties. If the spectra would be used to train a machine-learning algorithm (as is often done), either tissue slices with a single thickness would be needed (which is practically impossible in clinical practice), or much more data would be needed to train the algorithm to account for

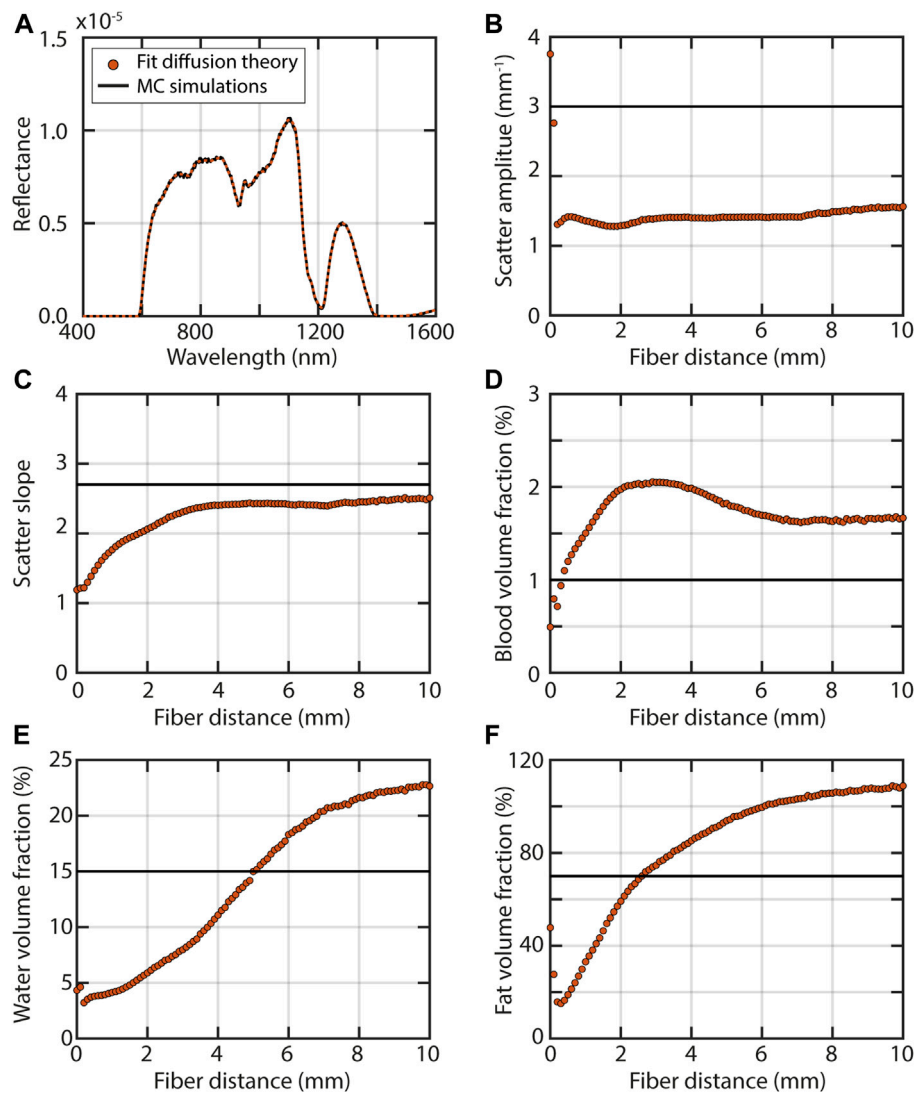


FIGURE 9

A pitfall in the development of diagnostic algorithms is not realizing that results from one fiber distance or spatial frequency cannot simply be translated to another fiber distance or spatial frequency. For example, when a diffusion theory model is used for fiber-optic measurements, the extracted optical properties will depend on the distance between the source and detector fiber. Results from Monte Carlo simulations for illumination through a fiber with a diameter of $200\ \mu\text{m}$ and an NA of 0.22 of a sample with optical properties representative of breast tissue (Jacques, 2013), where $\mu_s' = 3 \cdot (\lambda/500\ \text{nm})^{-2.7}$, a blood volume fraction of 1%, a fat volume fraction of 15% and a water volume fraction of 70%. The refractive index of the medium was 1.35 and above the medium 1.0. Detection was also through a fiber with a diameter of $200\ \mu\text{m}$ and an NA of 0.22, placed at several distances from the source fiber in increments of $100\ \mu\text{m}$. Black lines indicate the Monte Carlo simulations and red lines and circles the fit results for the diffusion theory model of (Farrell, Patterson and Wilson, 1992) (A) Example of a fit with diffusion theory to the simulated reflectance for a fiber distance of 10 mm. (B) Fit results and simulated value of the scattering amplitude (C) scattering slope (D) blood volume fraction (E) fat volume fraction; and (F) water volume fraction. The inaccuracies in all extracted optical properties over all fiber distances imply that diffusion theory does not hold for these simulated measurements, which can be explained by the fact that the ratio between the reduced scattering coefficient and the absorption coefficient is too low. The extracted optical properties change with fiber distance.

the additional influence of the slice thickness. Even in that case, the trained algorithm would not be translatable to *in vivo* applications, where the tissue in essence will be semi-infinite and thus the measured reflectance spectra would be different.

The fact that the interrogation depth varies with fiber distance or spatial frequency also offers the opportunity to

extract depth information on tissue optical properties. For example, fiber-optic probes with multiple fibers distances and SFDI with multiple frequencies have been used to extract optical properties of different tissue layers, as well as the thickness of the layers (Sharma et al., 2014; Tabassum et al., 2018; Geldof et al., 2022; Sung et al., 2022). Also, in the very first paper where SFDI

was presented (Cuccia et al., 2005), Cuccia et al. already suggested obtaining tomographic images of optical properties from images obtained with multiple spatial frequencies, and more recently methods have been developed to enable this (Konecky et al., 2009, 2012).

Diagnostic algorithms

Diagnostic algorithms are generally either based on tissue optical properties extracted from the measured spectra or on the entire spectra themselves. For diffuse measurements, analytical models exist to extract tissue optical properties from reflectance spectra (Flock et al., 1989; Farrell, Patterson and Wilson, 1992; Cuccia et al., 2009). For fiber-optic subdiffuse measurements, a semi-empirical model exists for SFR spectroscopy (Post A. L. et al., 2020), which applies when the source and detector fiber overlap. However, for measurements where the source and detector fiber do not overlap but are too close together for diffusion theory to apply, no model exists. For wide-field subdiffuse measurements, Kanick et al. developed a model, but this does not incorporate the influence of absorption on the measured spectra (Kanick et al., 2014). Both the SFR and SFDI models have been derived semi-empirically from MC simulations. Other approaches to extract tissue optical properties are based on look-up tables derived from MC simulations or measurements on phantoms (Hennessy et al., 2013; Vervandier and Gioux, 2013; Ivančić et al., 2018; Erickson, Durkin and Tunnell, 2022) or machine learning based on MC simulations (Chen et al., 2016; Ivančić et al., 2018; Stier et al., 2021). Since subdiffuse measurements are very sensitive to the tissue scattering phase function, simulations from which models or look-up tables are derived should be performed with a wide range of tissue scattering phase functions. Based on our review of tissue scattering phase functions, it should at least include TTHG and MHG phase functions, since these scattering phase function models are representative of measured phase functions in soft tissue. To ensure accurate results from subdiffuse measurements for any tissue type we would suggest also including phase functions based on Mie theory with a fractal size distribution, MPC phase functions (representative of blood) and RMC phase functions (representative of cells and dentin). The HG phase function should not be included, since it never represented the measured scattering phase functions well and it underestimates backward scattering. Previously MC simulation software was limited to HG phase functions only, but more recently MC software has become available where any scattering phase function can be implemented (e.g. MCX (Yu et al., 2018)). The importance of using a range of scattering phase functions for the development of a subdiffuse model was illustrated by (Post A. L. et al., 2020). They developed a model based on MC simulations with TTHG, MHG, RMC, and MPC phase functions and compared their accuracy for this range of phase functions to

the model previously developed by (Kanick et al., 2011), which was based only on MHG phase functions. Post et al. increased the accuracy of the model by a factor of 3. Thus, approaches to extract optical properties from subdiffuse measurements based on MC simulations with MHG phase functions alone are prone to errors.

Although counterintuitive, another approach to extract optical properties from subdiffuse measurements is to use diffusion theory—as has been done for fiber-optic measurements with short source-detector separations (Müller et al., 2003; de Boer et al., 2016). The extracted optical properties will not be accurate—even when diffusion theory only slightly underestimates the reflectance, this can lead to large errors in the extracted optical properties (Naglič et al., 2019). For clinical applications inaccuracies in the extracted optical properties are not necessarily a problem as long as the extracted optical properties are reproducible.

Figure 9 shows what can happen when a diffuse model is used for fiber-optic reflectance measurements of breast tissue. For this specific example, diffusion theory is not appropriate regardless of the fiber distance, because the absorption coefficient is much higher than the reduced scattering coefficient for part of the spectrum due to the presence of fat and water. For short fiber distances, the volume fractions of blood, fat, and water are underestimated. This underestimation can be explained by the fact that the reflectance close to the source is higher than expected based on diffusion theory (Figure 2A) which can be accounted for by a lower absorption. The scatter amplitude is fairly constant but inaccurate regardless of the fiber distance. The scatter slope does become increasingly accurate with fiber distance. Interestingly, further away from the source the extracted concentrations of absorbers are still inaccurate, but there they are overestimated. The inaccuracies in the scattering amplitude and the volume fraction of absorbers can be explained by the fact that the reduced scattering coefficient should be much larger than the absorption coefficient for diffusion theory to apply. For this simulated breast tissue, this is not the case at higher wavelengths.

Figure 9 thus illustrates an important pitfall in diagnostic algorithm development: not realizing that results from one fiber distance or spatial frequency cannot be translated to another one. When a fit with diffusion theory is performed in the subdiffuse regime, the fiber distance or spatial frequency will influence the values of the extracted optical properties that are used in a diagnostic algorithm. When machine learning is used, the features that were used by the diagnostic algorithm for one fiber distance or spatial frequency will not necessarily perform equally well for other fiber distances. Also, when tissue is not homogenous but layered, diagnostic algorithms from different fiber distances or spatial frequencies are definitely not interchangeable, since they will have interrogated different volumes and thus different layers of different tissue types.

Tissue scattering phase function

Knowledge of tissue scattering phase functions is important for both modeling and interpretation of subdiffuse measurements. However, currently, we cannot be sure that the MHG, TTHG, Mie for a fractal size distribution, RMC, and MPC are sufficient to fully describe all phase functions that are present in tissue. First of all, only a small number of tissue scattering phase functions have been measured (29) for only a small number of tissue types (13). Secondly, most scattering phase functions were only measured up to 150° and we thus do not know if the currently used phase function models accurately describe small angle backscattering events—which have a major impact on subdiffuse measurements. To better understand the tissue scattering phase function to improve our understanding of subdiffuse techniques, we thus need new approaches that can cover the full range of scattering angles, and we need more measurements of scattering phase functions of different tissue types.

We also need a better understanding of how the tissue scattering phase function relates to the disease state of tissue. Some work has been done that relates the scattering phase function to the subcellular structure of tissue, but we do not yet know how the tissue scattering phase function changes from healthy to diseased tissue. Only (Ghosh et al., 2001) measured the scattering phase function of both normal and malignant (breast) tissue. Furthermore, we do not know how subdiffuse parameters such as p_{sb} relate to changes in the tissue structure. To obtain a better understanding of p_{sb} , subdiffuse measurements of p_{sb} could be related to histology slides of the investigated tissue.

Conclusion

For steady-state reflectance spectroscopy, the tissue optical properties and the distance between source and detector fibers or the projected spatial frequency determine whether measurements are in the diffuse or subdiffuse regime. When fiber distances are too short or spatial frequencies too high for diffusion theory to apply, these measurements are in the so-called subdiffuse regime. The fiber distance or spatial frequency has important implications for clinical applications of reflectance spectroscopy since they influence which tissue optical properties the technique is sensitive to and the size of the tissue volume that is interrogated. An opportunity in reflectance spectroscopy is that the interrogation depth can be tailored to a clinical application by appropriate selection of a fiber distance or spatial frequency. Another opportunity in

reflectance spectroscopy is the sensitivity of subdiffuse measurements to the tissue scattering phase function—which has the potential to be a powerful contrast mechanism between healthy and diseased tissue. A pitfall in reflectance spectroscopy is not properly considering the effect of the interrogation depth on a clinical measurement and not realizing the variable interrogation depth within a spectrum. Another pitfall is assuming diagnostic algorithms developed from measurements with a certain fiber distance or spatial frequency can be used for measurements with another fiber distance or spatial frequency. Lastly, an important pitfall is developing models to extract optical properties from subdiffuse measurements based on MC simulations that do not cover the full range of phase functions present in tissue (at least modified Henyey-Greenstein and two-term Henyey-Greenstein should be included).

Author contributions

AP conceived the study. All authors contributed to the design of the study. MW and AP performed the analyses and wrote the manuscript. All authors contributed to manuscript revision, read, and approved the submitted version.

Funding

Nederlandse Organisatie voor Wetenschappelijk Onderzoek—17908.

Conflict of interest

The authors declare that the research was conducted in the absence of any commercial or financial relationships that could be construed as a potential conflict of interest.

Publisher's note

All claims expressed in this article are solely those of the authors and do not necessarily represent those of their affiliated organizations, or those of the publisher, the editors and the reviewers. Any product that may be evaluated in this article, or claim that may be made by its manufacturer, is not guaranteed or endorsed by the publisher.

References

Akter, S., Hossain, M. G., Nishidate, I., Hazama, H., and Awazu, K. (2018). Medical applications of reflectance spectroscopy in the diffusive and sub-diffusive regimes. *J. Near Infrared Spectrosc.* 26 (6), 337–350. doi:10.1177/0967033518806637

Arnfield, M. R., Tulip, J., and Mcphee, M. S. (1988). Optical propagation in tissue with anisotropic scattering. *IEEE Trans. Biomed. Eng.* 35 (5), 372–381. doi:10.1109/10.1396

- Bevilacqua, F., and Deppeursinge, C. (1999). Monte Carlo study of diffuse reflectance at source-detector separations close to one transport mean free path. *J. Opt. Soc. Am. A* 16 (12), 2935–2945. doi:10.1364/JOSAA.16.002935
- Bodenschatz, N., Krauter, P., Liemert, A., and Kienle, A. (2016). Quantifying phase function influence in subdiffusively backscattered light. *J. Biomed. Opt.* 21 (3), 035002. doi:10.1117/1.JBO.21.3.035002
- Bodenschatz, N., Krauter, P., Liemert, A., Wiest, J., and Kienle, A. (2015). Model-based analysis on the influence of spatial frequency selection in spatial frequency domain imaging. *Appl. Opt.* 54 (22), 6725–6731. doi:10.1364/AO.54.006725
- Bruls, W. A. G., and Van Der Leun, J. C. (1984). Forward scattering properties of human epidermal layers. *Photochem. Photobiol.* 40 (2), 231–242. doi:10.1111/j.1751-1097.1984.tb04581.x
- Bugter, O., Hardillo, J. A., Baatenburg de Jong, R. J., Amelink, A., and Robinson, D. J. (2018). Optical pre-screening for laryngeal cancer using reflectance spectroscopy of the buccal mucosa. *Biomed. Opt. Express* 9 (10), 4665. doi:10.1364/boe.9.004665
- Bugter, O., Spaander, M. C. W., Bruno, M. J., de Jong, R. J. B., Amelink, A., and Robinson, D. J. (2018). Optical detection of field cancerization in the buccal mucosa of patients with esophageal cancer. *Clin. Transl. Gastroenterol.* 9 (4), e152. doi:10.1038/s41424-018-0023-6
- Bugter, O., van Brummelen, S., van der Leest, K., Aerts, J., Maat, A., Baatenburg de Jong, R., et al. (2019). Towards the optical detection of field cancerization in the buccal mucosa of patients with lung cancer. *Transl. Oncol.* 12 (12), 1533–1538. doi:10.1016/j.tranon.2019.07.018
- Calabro, K. W., and Bigio, I. J. (2014). Influence of the phase function in generalized diffuse reflectance models: Review of current formalisms and novel observations. *J. Biomed. Opt.* 19 (7), 075005. doi:10.1117/1.JBO.19.7.075005
- Canpolat, M., and Mourant, J. R. (2000). High-angle scattering events strongly affect light collection in clinically relevant measurement geometries for light transport through tissue. *Phys. Med. Biol.* 45, 1127–1140. doi:10.1088/0031-9155/45/5/304
- Chen, Y.-W., Chen, C. C., Huang, P. J., and Tseng, S. H. (2016). Artificial neural networks for retrieving absorption and reduced scattering spectra from frequency-domain diffuse reflectance spectroscopy at short source-detector separation. *Biomed. Opt. Express* 7 (4), 1496–1510. doi:10.1364/boe.7.001496
- Cuccia, D. J., Bevilacqua, F., Durkin, A. J., Ayers, F. R., and Tromberg, B. J. (2009). Quantitation and mapping of tissue optical properties using modulated imaging. *J. Biomed. Opt.* 14 (2), 024012. doi:10.1117/1.3088140
- Cuccia, D. J., Bevilacqua, F., Durkin, A. J., and Tromberg, B. J. (2005). Modulated imaging: Quantitative analysis and tomography of turbid media in the spatial-frequency domain. *Opt. Lett.* 30 (11), 1354–1356. doi:10.1364/ol.30.001354
- Curtius, K., Wright, N. A., and Graham, T. A. (2017). An evolutionary perspective on field cancerization. *Nat. Rev. Cancer* 18 (1), 19–32. doi:10.1038/nrc.2017.102
- de Boer, L. L., Hendriks, B. H. W., van Duijnhoven, F., Peeters-Baas, M. J. T. F. D. V., Van de Vijver, K., Loo, C. E., et al. (2016). Using DRS during breast conserving surgery: Identifying robust optical parameters and influence of inter-patient variation. *Biomed. Opt. Express* 7 (12), 5188–5200. doi:10.1364/BOE.7.005188
- Drezek, R., Dunn, A., and Richards-Kortum, R. (1999). Light scattering from cells: Finite-difference time-domain simulations and goniometric measurements. *Appl. Opt.* 38 (16), 3651–3661. doi:10.1364/ao.38.003651
- Erickson, T. A., Durkin, A. J., and Tunnell, J. W. (2022). Lookup-table method for imaging optical properties with structured illumination beyond the diffusion theory regime. *J. Biomed. Opt.* 15 (3), 036013. doi:10.1117/1.3431728
- Faber, D. J., Post, A. L., Sterenberg, H. J. C. M., and Van Leeuwen, T. G. (2019). Analytical model for diffuse reflectance in single fiber reflectance spectroscopy. *Opt. Lett.* 45 (7), 2078–2081. doi:10.1364/ol.385845
- Farrell, T. J., Patterson, M. S., and Wilson, B. (1992). A diffusion theory model of spatially resolved, steady-state diffuse reflectance for the noninvasive determination of tissue optical properties *in vivo*. *Med. Phys.* 19 (4), 879–888. doi:10.1118/1.596777
- Fawzy, Y. S., Petek, M., Terceelj, M., and Zeng, H. (2006). *In vivo* assessment and evaluation of lung tissue morphologic and physiological changes from non-contact endoscopic reflectance spectroscopy for improving lung cancer detection. *J. Biomed. Opt.* 11 (4), 044003. doi:10.1117/1.2337529
- Firbank, M., Hiraoka, M., Essenpreis, M., and Delpy, D. T. (1993). Measurement of the optical properties of the skull in the wavelength range 650–950 nm. *Phys. Med. Biol.* 38 (4), 503–510. doi:10.1088/0031-9155/38/4/002
- Flock, S. T., Patterson, M., Wilson, B., and Wyman, D. (1989). Monte Carlo modeling of light propagation in highly scattering tissues—I: Model predictions and comparison with diffusion theory. *IEEE Trans. Biomed. Eng.* 36 (12), 1162–1168. doi:10.1109/TBME.1989.1173624
- Forster, F. K., Kienle, A., Michels, R., and Hibst, R. (2006). Phase function measurements on nonspherical scatterers using a two-axis goniometer. *J. Biomed. Opt.* 11 (2), 024018. doi:10.1117/1.2187421
- Gamm, U. A., Kanick, S. C., Sterenberg, H. J. C. M., Robinson, D. J., and Amelink, A. (2012). Quantification of the reduced scattering coefficient and phase-function-dependent parameter γ of turbid media using multidiameter single fiber reflectance spectroscopy: Experimental validation. *Opt. Lett.* 37 (11), 1838–1840. doi:10.1364/OL.37.001838
- Gareau, D. S. (2006). *In vivo* confocal microscopy in turbid media. Available at: <https://digitalcollections.ohsu.edu/concern/etds/pz50gw084?locale=en>.
- Geldof, F., Dashtbozorg, B., Hendriks, B. H. W., Sterenberg, H. J. C. M., and Ruers, T. J. M. (2022). Layer thickness prediction and tissue classification in two-layered tissue structures using diffuse reflectance spectroscopy. *Sci. Rep.* 12 (1), 1698. doi:10.1038/s41598-022-05751-5
- Ghosh, N., Mohanty, S. K., Majumder, S. K., and Gupta, P. K. (2001). Measurement of optical transport properties of normal and malignant human breast tissue. *Appl. Opt.* 40 (1), 176–184. doi:10.1364/AO.40.000176
- Gioux, S., Mazhar, A., and Cuccia, D. J. (2019). Spatial frequency domain imaging in 2019: Principles, applications, and perspectives. *J. Biomed. Opt.* 24 (07), 1. doi:10.1117/1.JBO.24.7.071613
- Hammer, M., Yaroslavsky, A. N., and Schweitzer, D. (2001). A scattering phase function for blood with physiological hematocrit. *Phys. Med. Biol.* 46 (3), N65–N69. doi:10.1088/0031-9155/46/3/402
- Hayakawa, C. K., Karrobi, K., Pera, V., Roblyer, D., and Venugopalan, V. (2018). Optical sampling depth in the spatial frequency domain. *J. Biomed. Opt.* 24 (7), 1. doi:10.1117/1.JBO.24.7.071603
- Hennessy, R., Goth, W., Sharma, M., Markey, M. K., and Tunnell, J. W. (2014). Effect of probe geometry and optical properties on the sampling depth for diffuse reflectance spectroscopy. *J. Biomed. Opt.* 19 (10), 107002. doi:10.1117/1.jbo.19.10.107002
- Hennessy, R., Lim, S. L., Markey, M. K., and Tunnell, J. W. (2013). Monte Carlo lookup table-based inverse model for extracting optical properties from tissue-simulating phantoms using diffuse reflectance spectroscopy. *J. Biomed. Opt.* 18 (3), 037003. doi:10.1117/1.jbo.18.3.037003
- Ivančić, M., Naglic, P., Pernus, F., Likar, B., and Burmen, M. (2018). Efficient estimation of subdiffusive optical parameters in real time from spatially resolved reflectance by artificial neural networks. *Opt. Lett.* 43 (12), 2901. doi:10.1364/ol.43.002901
- Jacques, S. L., Alter, C. A., and Prah, S. A. (1987). Angular dependence of HeNe laser light scattering by human dermis. *Lasers Life Sci.* 1 (4), 309–333.
- Jacques, S. L. (2013). Corrigendum: Optical properties of biological tissues: A review. *Phys. Med. Biol.* 58 (14), 5007–5008. doi:10.1088/0031-9155/58/14/5007
- Jansen-Winkeln, B., Holfert, N., Kohler, H., Moulla, Y., Takoh, J. P., Rabe, S. M., et al. (2019). Determination of the transection margin during colorectal resection with hyperspectral imaging (HSI). *Int. J. Colorectal Dis.* 34 (4), 731–739. doi:10.1007/s00384-019-03250-0
- Kanick, S. C., Gamm, U. A., Sterenberg, H. J. C. M., Robinson, D. J., and Amelink, A. (2011). Method to quantitatively estimate wavelength-dependent scattering properties from multidiameter single fiber reflectance spectra measured in a turbid medium. *Opt. Lett.* 36 (15), 2997–2999. doi:10.1364/ol.36.002997
- Kanick, S. C., McClatchy, D. M., Krishnaswamy, V., Elliott, J. T., Paulsen, K. D., and Pogue, B. W. (2014). Sub-diffusive scattering parameter maps recovered using wide-field high-frequency structured light imaging. *Biomed. Opt. Express* 5 (10), 3376. doi:10.1364/boe.5.003376
- Kanick, S. C., Robinson, D. J., Sterenberg, H. J. C. M., and Amelink, A. (2009). Monte Carlo analysis of single fiber reflectance spectroscopy: Photon path length and sampling depth. *Phys. Med. Biol.* 54, 6991–7008. doi:10.1088/0031-9155/54/22/016
- Kho, E., Boer, L. L., Post, A. L., Van de Vijver, K. K., Jozwiak, K., Sterenberg, H. J., et al. (2019b). Imaging depth variations in hyperspectral imaging: Development of a method to detect tumor up to the required tumor-free margin width. *J. Biophot.* 12 (11), e201900086. doi:10.1002/jbio.201900086
- Kho, E., de Boer, L. L., Van de Vijver, K. K., van Duijnhoven, F., Vrancken Peeters, M. J. T., Sterenberg, H. J., et al. (2019a). Hyperspectral imaging for resection margin assessment during cancer surgery. *Clin. Cancer Res.* 25 (12), 3572–3580. doi:10.1158/1078-0432.CCR-18-2089
- Konecky, S. D., Mazhar, A., Cuccia, D., Durkin, A. J., Schotland, J. C., and Tromberg, B. J. (2009). Quantitative optical tomography of sub-surface heterogeneities using spatially modulated structured light. *Opt. Express* 17 (17), 14780. doi:10.1364/oe.17.014780

- Konecky, S. D., Owen, C. M., Rice, T., Valde's, P. A., Kolste, K., Wilson, B. C., et al. (2012). Spatial frequency domain tomography of protoporphyrin IX fluorescence in preclinical glioma models. *J. Biomed. Opt.* 17 (5), 056008. doi:10.1117/1.jbo.17.5.056008
- Lin, J., Clancy, N. T., Qi, J., Hu, Y., Tatla, T., Stoyanov, D., et al. (2018). Dual-modality endoscopic probe for tissue surface shape reconstruction and hyperspectral imaging enabled by deep neural networks. *Med. Image Anal.* 48, 162–176. doi:10.1016/j.media.2018.06.004
- Lin, S.-P., Wang, L., Jacques, S. L., and Tittel, F. K. (1997). Measurement of tissue optical properties by the use of oblique-incidence optical fiber reflectometry. *Appl. Opt.* 36 (1), 136. doi:10.1364/ao.36.00136
- Lu, G., and Fei, B. (2014). Medical hyperspectral imaging: A review. *J. Biomed. Opt.* 19 (1), 010901. doi:10.1117/1.JBO.19.1.010901
- Marchesini, R., Bertoni, A., Andreola, S., Melloni, E., and Sichirillo, A. E. (1989). Extinction and absorption coefficients and scattering phase functions of human tissues *in vitro*. *Appl. Opt.* 28 (12), 2318. doi:10.1364/ao.28.002318
- Martelli, F., Del Bianco, S., Ismaelli, A., and Zaccanti, G. (2009). *Light propagation through biological tissue and other diffusive media: Theory, solutions, and software*. Bellingham, Washington: SPIE. doi:10.1117/12.2283590
- McClatchy, D. M., Rizzo, E. J., Wells, W. A., Black, C. C., Paulsen, K. D., Kanick, S. C., et al. (2018). Light scattering measured with spatial frequency domain imaging can predict stromal versus epithelial proportions in surgically resected breast tissue. *J. Biomed. Opt.* 24 (7), 1. doi:10.1117/1.jbo.24.7.071605
- McClatchy, D. M., Rizzo, E. J., Wells, W. A., Cheney, P. P., Hwang, J. C., Paulsen, K. D., et al. (2016). Wide-field quantitative imaging of tissue microstructure using sub-diffuse spatial frequency domain imaging. *Optica* 3 (6), 613. doi:10.1364/optica.3.000613
- Momi, N., Backman, V., Brendler, C. B., and Roy, H. K. (2015). Harnessing novel modalities: Field carcinogenesis detection for personalizing prostate cancer management. *Future Oncol.* 11 (20), 2737–2741. doi:10.2217/fo.15.182
- Mourant, J. R., Boyer, J., Hielscher, A. H., and Bigio, I. J. (1996). Influence of the scattering phase function on light transport measurements in turbid media performed with small source-detector separations. *Opt. Lett.* 21 (7), 546–548. doi:10.1364/OL.21.000546
- Mourant, J. R., Canpolat, M., Brocker, C., Esponda-Ramos, O., Johnson, T. M., Matanock, A., et al. (2000). Light scattering from cells: The contribution of the nucleus and the effects of proliferative status. *J. Biomed. Opt.* 5 (2), 131–137. doi:10.1117/1.429979
- Mourant, J. R., Freyer, J. P., Hielscher, A. H., Eick, A. A., Shen, D., and Johnson, T. M. (1998). Mechanisms of light scattering from biological cells relevant to noninvasive optical-tissue diagnostics. *Appl. Opt.* 37 (16), 3586. doi:10.1364/AO.37.003586
- Müller, M. G., Valdez, T. A., Georgakoudi, I., Backman, V., Fuentes, C., Kabani, S., et al. (2003). Spectroscopic detection and evaluation of morphologic and biochemical changes in early human oral carcinoma. *Cancer* 97 (7), 1681–1692. doi:10.1002/cncr.11255
- Naglić, P., Pernuš, F., Likar, B., and Bürmen, M. (2017). “Estimation of optical properties from subdiffusive reflectance beyond the second similarity parameter γ ,” in *Diffuse optical spectroscopy and imaging VI* (Bellingham, Washington: SPIE), 1041205. doi:10.1117/12.2286344
- Naglić, P., Pernuš, F., Likar, B., and Burmen, M. (2016). Estimation of optical properties by spatially resolved reflectance spectroscopy in the subdiffusive regime. *J. Biomed. Opt.* 21 (9), 095003. doi:10.1117/1.JBO.21.9.095003
- Naglić, P., Vidovic, L., Milanic, M., Randeberg, L. L., and Majaron, B. (2019). Suitability of diffusion approximation for an inverse analysis of diffuse reflectance spectra from human skin *in vivo*. *OSA Contin.* 2 (3), 905. doi:10.1364/osac.2.000905
- Okamoto Ugnell, A., and Öberg, P. Å. (1997). The optical properties of the cochlear bone. *Med. Eng. Phys.* 19 (7), 630–636. doi:10.1016/S1350-4533(97)00015-5
- O'Sullivan, T. D., Cerussi, A. E., Cuccia, D. J., and Tromberg, B. J. (2012). Diffuse optical imaging using spatially and temporally modulated light. *J. Biomed. Opt.* 17 (7), 0713111. doi:10.1117/1.jbo.17.7.071311
- Pfeiffer, N., and Chapman, G. H. (2008). Successive order, multiple scattering of two-term Henyey-Greenstein phase functions. *Opt. Express* 16 (18), 13637–13642. doi:10.1364/OE.16.013637
- Piao, D., and Patel, S. (2017). Simple empirical master-slave dual-source configuration within the diffusion approximation enhances modeling of spatially resolved diffuse reflectance at short-path and with low scattering from a semi-infinite homogeneous medium. *Appl. Opt.* 56 (5), 1447. doi:10.1364/AO.56.001447
- Post, A. L., Sterenborg, H. J. C. M., Woltjer, F. G., van Leeuwen, T. G., and Faber, D. J. (2020a). Subdiffuse scattering model for single fiber reflectance spectroscopy. *J. Biomed. Opt.* 25 (1), 1. doi:10.1117/1.JBO.25.1.015001
- Post, A. L., Faber, D. J., Sterenborg, H. J. C. M., and van Leeuwen, T. G. (2020b). Subdiffuse scattering and absorption model for single fiber reflectance spectroscopy. *Biomed. Opt. Express* 11 (11), 6620. doi:10.1364/BOE.402466
- Post, A. L., Groof, A. J., Zhang, X. U., Swager, A., Fockens, K. N., Pouw, R. E., et al. (2021). Toward improved endoscopic surveillance with multidiameter single fiber reflectance spectroscopy in patients with Barrett's esophagus. *J. Biophot.* 14 (4), e202000351. doi:10.1002/jbio.202000351
- Post, A. L., Jacques, S. L., Sterenborg, H. J. C. M., Faber, D. J., and van Leeuwen, T. G. (2017). Modeling subdiffusive light scattering by incorporating the tissue phase function and detector numerical aperture. *J. Biomed. Opt.* 22 (5), 050501. doi:10.1117/1.JBO.22.5.050501
- Prahl, S. A. (1989). “A Monte Carlo model of light propagation in tissue,” in *Dosimetry of laser radiation in medicine and biology* (Bellingham, Washington: SPIE), 1030509. doi:10.1117/12.2283590
- Radosevich, A. J., Mutyal, N. N., Yi, J., Stypula-Cyrus, Y., Rogers, J. D., Goldberg, M. J., et al. (2013). Ultrastructural alterations in field carcinogenesis measured by enhanced backscattering spectroscopy. *J. Biomed. Opt.* 18 (9), 097002. doi:10.1117/1.JBO.18.9.097002
- Reynolds, L. O., and McCormick, N. J. (1980). Approximate two-parameter phase function for light scattering. *J. Opt. Soc. Am.* 70 (10), 1206–1212. doi:10.1364/JOSA.70.001206
- Roy, H. K., Turzhitsky, V., Kim, Y., Goldberg, M. J., Watson, P., Rogers, J. D., et al. (2009). Association between rectal optical signatures and colonic neoplasia: Potential applications for screening. *Cancer Res.* 69 (10), 4476–4483. doi:10.1158/0008-5472.CAN-08-4780
- Saccomandi, P., Vogel, V., Bazrafshan, B., Maurer, J., Schena, E., Vogl, T. J., et al. (2015). Estimation of anisotropy coefficient of swine pancreas, liver and muscle at 1064 nm based on goniometric technique. *J. Biophot.* 8 (5), 422–428. doi:10.1002/jbio.201400057
- Sharma, M., Hennessy, R., Markey, M. K., and Tunnell, J. W. (2014). Verification of a two-layer inverse Monte Carlo absorption model using multiple source-detector separation diffuse reflectance spectroscopy. *Biomed. Opt. Express* 5 (1), 40–53. doi:10.1364/boe.5.000040
- Stegehuis, P. L., Boogerd, L. S. F., Inderson, A., Veenendaal, R. A., van Gerven, P., Bonsing, B. A., et al. (2017). Toward optical guidance during endoscopic ultrasound-guided fine needle aspirations of pancreatic masses using single fiber reflectance spectroscopy: A feasibility study. *J. Biomed. Opt.* 22 (2), 024001. doi:10.1117/1.JBO.22.2.024001
- Stewart, S., Darr, M., Gomer, H., Smith, A., Samiei, A., Post, J. C., et al. (2020). Visible near infrared reflectance molecular chemical imaging of human *ex vivo* carcinomas and murine *in vivo* carcinomas. *J. Biomed. Opt.* 25 (02), 1. doi:10.1117/1.jbo.25.2.026003
- Stier, A. C., Goth, W., Hurley, A., Brown, T., Feng, X., Zhang, Y., et al. (2021). Imaging sub-diffuse optical properties of cancerous and normal skin tissue using machine learning-aided spatial frequency domain imaging. *J. Biomed. Opt.* 26 (9), 096007. doi:10.1117/1.jbo.26.9.096007
- Streeter, S. S., Maloney, B. W., Zuurbier, R. A., Wells, W. A., Barth, R. J., Paulsen, K. D., et al. (2021). Optical scatter imaging of resected breast tumor structures matches the patterns of micro-computed tomography. *Phys. Med. Biol.* 66 (11), 115021. doi:10.1088/1361-6560/ac01f1
- Sung, K., Shih, K. W., Hsu, F. W., Hsieh, H. P., Chuang, M. J., Hsiao, Y. H., et al. (2022). Accurate extraction of optical properties and top layer thickness of two-layered mucosal tissue phantoms from spatially resolved reflectance spectra. *J. Biomed. Opt.* 19 (7), 077002. doi:10.1117/1.jbo.19.7.077002
- Tabassum, S., Pera, V., Greening, G., Muldoon, T. J., and Roblyer, D. (2018). Two-layer inverse model for improved longitudinal preclinical tumor imaging in the spatial frequency domain. *J. Biomed. Opt.* 23 (7), 076011. doi:10.1117/1.JBO.23.7.076011
- Taddeucci, A., Martelli, F., Barilli, M., Ferrari, M., and Zaccanti, G. (1996). Optical Properties of brain tissue. *J. Biomed. Opt.* 1 (1), 117–123. doi:10.1117/12.227816
- Tian, H., Liu, Y., and Wang, L. (2006). Influence of the third-order parameter on diffuse reflectance at small source-detector separations. *Opt. Lett.* 31 (7), 933–935. doi:10.1364/OL.31.000933
- Utzing, U., and Richards-Kortum, R. R. (2003). Fiber optic probes for biomedical optical spectroscopy. *J. Biomed. Opt.* 8 (1), 121–147. doi:10.1117/1.1528207
- van der Zee, P., Essenpreis, M., and Delpy, D. T. (1993). “Optical properties of brain tissue,” in *Photon migration and imaging in random media and tissues* (Bellingham, Washington: SPIE), 454–465. doi:10.1117/12.154665
- Vervandier, J., and Gioux, S. (2013). Single snapshot imaging of optical properties. *Biomed. Opt. Express* 4 (12), 2938–2944. doi:10.1364/BOE.4.002938

- Vitkin, E., Turzhitsky, V., Qiu, L., Guo, L., Itzkan, I., Hanlon, E. B., et al. (2011). Photon diffusion near the point-of-entry in anisotropically scattering turbid media. *Nat. Commun.* 2 (1), 587. doi:10.1038/ncomms1599
- Wang, L. V., Jacques, S. L., and Zheng, L. (1995). Monte Carlo modeling of light transport in tissues. *Comput. Methods Programs Biomed.* 47, 73–100. doi:10.1007/978-1-4757-6092-7_4
- Wang, R. K. (2000). Modelling optical properties of soft tissue by fractal distribution of scatterers. *J. Mod. Opt.* 47 (1), 103–120. doi:10.1080/09500340008231409
- Wietlicka-piszc, M., Mazur, R., and Grzegorzewski, B. (1994). “Goniometric investigations of light scattered by bones of the skull,” in Proceedings of SPIE (Bellingham, Washington: SPIE). doi:10.1117/12.192028
- Xu, M. (2016). Diagnosis of the phase function of random media from light reflectance. *Sci. Rep.* 6 (2), 22535–22537. doi:10.1038/srep22535
- Xu, M., Wu, T. T., and Qu, J. Y. (2008). Unified Mie and fractal scattering by cells and experimental study on application in optical characterization of cellular and subcellular structures. *J. Biomed. Opt.* 13 (2), 024015. doi:10.1117/1.2907790
- Yaroslavskaia, A. N., Utz, S. R., Tatarintsev, S. N., and Tuchin, V. V. (1994). “Angular scattering properties of human epidermal layers,” in Proceedings of SPIE (Bellingham, Washington: SPIE), 2100. doi:10.1117/12.179025
- Yaroslavsky, A. N., Yaroslavsky, I. V., Goldbach, T., and Schwarzmaier, H. J. (1996). Optical properties of blood in the near-infrared spectral range. *Proc. SPIE - Int. Soc. Opt. Eng.* 2678 (5), 314–324. doi:10.1117/12.239516
- Yu, L., Nina-Paravecino, F., Kaeli, D., and Fang, Q. (2018). Scalable and massively parallel Monte Carlo photon transport simulations for heterogeneous computing platforms. *J. Biomed. Opt.* 23 (1), 1. doi:10.1117/1.jbo.23.1.010504
- Zijp, J. R., and ten Bosch, J. J. (1994). Use of tabulated cumulative density functions to generate pseudorandom numbers obeying specific distributions for Monte Carlo simulations. *Appl. Opt.* 33 (3), 533–534. doi:10.1364/AO.33.000533
- Zijp, J., and ten Bosch, J. (1998). Optical properties of bovine muscle tissue *in vitro*; a comparison of methods. *Phys. Med. Biol.* 43 (10), 3065–3081. doi:10.1088/0031-9155/43/10/026